study. These factors together may have obscured the TIMP-1–inducing property of VS in this study.

Clinical Implication

Early short-term VS strategy appears to be clinically feasible in patients with acute MI. Furthermore, this strategy may be both timely and sufficient based on the following evidence. First, upregulation of plasma and myocardial TNF-α as well as myocardial infiltration of neutrophils are mostly confined to within 3 days after MI.[15,37] Meanwhile, the anti-inflammatory effects of VS are long-lasting. In mice, only 30 seconds of VS significantly suppressed TNF-α activation in response to lipopolysaccharide challenge even at 48 hours after VS.[11] Second, pharmacological inhibition of MMP activity for 48 hours after MI preserves the original extracellular matrix, thereby lessens LV remodeling.[18]

Although the present findings suggest clinically useful strategy of VS, several issues remain to be solved before VS can be considered for clinical application in patients with MI. First, it is unclear whether VS is able to provide additional therapeutic benefits to current pharmacological treatments such as renin-angiotensin-aldosterone inhibition or β-blockade, the efficacy of which has been well established in patients with MI.[38] Second, it is unclear whether VS started after reperfusion is also capable of attenuating LV remodeling after MI. Although we started VS during coronary occlusion in this study, initiating VS after coronary reperfusion may simulate a more clinically relevant situation, because prompt reperfusion of occluded coronary artery is given the utmost priority in the management of patients with acute MI. Further studies to solve these problems are clearly required.

VS did not afford any survival benefit in this study, which is inconsistent with previous findings that VS improves acute[7] or chronic[3] survival in rats after MI by preventing malignant arrhythmia and heart failure. However, the mortality rate in MI rats was ~60% within the first 24 hours in the previous study,[3] which is undoubtedly higher than that seen in MI rabbits of this study (~30%). Low mortality rate in MI rabbits may have masked the impact of VS on survival in this study.

Limitation

We focused on the antiremodeling effects of VS but did not include a detailed mechanistic investigation into how VS reduces LV infarct size. Inflammatory responses to MI play a significant role in determining the infarct size.[9] On the other hand, the infarct size, which reflects the degree of myocardial necrosis, is also one of the determinants of post-MI inflammatory reactions. Therefore, direct cardiomyocyte protection of VS possibly through the muscarinic acetylcholine pathway and the anti-inflammatory effect possibly through the nicotinic pathway may have contributed synergistically to the infarct size-reducing effect of VS. Selective inhibition of the muscarinic and nicotinic pathway by atropine and methyllycaconitine,[39] respectively, may allow elucidation of how these different mechanisms contribute to the beneficial effects of VS in a reperfused MI model. Further studies on these issues are clearly required.

Acute surgical trauma associated with open-chest preparation may have exaggerated the expression of CRP and TNF-α in MI and MI-VS rabbits in this study. For a more rational comparison of acute inflammatory reactions among NC, MI, and MI-VS animals, use of sham-operated rabbits as NC would be more appropriate. Closed-chest animal models of myocardial ischemia-reperfusion[40] may be an alternative to eliminate acute surgical trauma and allow assessment of inflammation strictly from myocardial injury. In this study, MI and MI-VS rabbits underwent identical surgical preparation. Therefore, it is fair to say that the difference in TNF-α expression in infarcts between the MI and MI-VS groups was valid in the present study.

In conclusion, early short-term VS attenuated cardiac dysfunction and myocardial structural remodeling in a rabbit model of reperfused MI. The beneficial effects of VS were associated with suppression of excessive TNF-α activation and myocardial infiltrations of neutrophils.

Acknowledgments

We thank Dr. Takeshi Aiba for his helpful comments on this manuscript.

Disclosures

Supported by Grant-in-Aid for Scientific Research from the Ministry of Education, Culture, Sports, Science and Technology (C-20500404 to K.U.), by a research grant from Nakatani Foundation of Electronic Measuring Technology Advancement (to K.U.), and by Health and Labour Sciences Research Grants from the Ministry of Health, Labour and Welfare of Japan (H19-nano-ippan-009 to M.S.).

References

1. Bolognese L, Cerisano G. Early predictors of left ventricular remodeling after acute myocardial infarction. Am Heart J 1999;138:S79–83.
2. Ezekowitz JA, Kaul P, Bakal JA, Armstrong PW, Welsh RC, McAlister FA. Declining in-hospital mortality and increasing heart failure incidence in elderly patients with first myocardial infarction. J Am Coll Cardiol 2009;53:13–20.
3. Li M, Zheng C, Sato T, Kawada T, Sugimachi M, Sunagawa K. Vagal nerve stimulation markedly improves long-term survival after chronic heart failure in rats. Circulation 2004;109:120–4.
4. Schwartz PJ, De Ferrari GM, Sanzo A, Landolina M, Rordorf R, Raineri C, et al. Long term vagal stimulation in patients with advanced heart failure: first experience in man. Eur J Heart Fail 2008;10:884–91.
5. Katare RG, Ando M, Kakinuma Y, Arikawa M, Handa T, Yamasaki F, et al. Vagal nerve stimulation prevents reperfusion injury through inhibition of opening of mitochondrial permeability transition pore independent of the bradycardiac effect. J Thorac Cardiovasc Surg 2009; 137:223–31.

6. Kawada T, Yamazaki T, Akiyama T, Kitagawa H, Shimizu S, Mizuno M, et al. Vagal stimulation suppresses ischemia-induced myocardial interstitial myoglobin release. Life Sci 2008;83:490–5.
7. Mioni C, Bazzani C, Giuliani D, Altavilla D, Leone S, Ferrari A, et al. Activation of an efferent cholinergic pathway produces strong protection against myocardial ischemia/reperfusion injury in rats. Crit Care Med 2005;33:2621–8.
8. Sun M, Dawood F, Wen WH, Chen M, Dixon I, Kirshenbaum LA, et al. Excessive tumor necrosis factor activation after infarction contributes to susceptibility of myocardial rupture and left ventricular dysfunction. Circulation 2004;110:3221–8.
9. Vinten-Johansen J. Involvement of neutrophils in the pathogenesis of lethal myocardial reperfusion injury. Cardiovasc Res 2004;61: 481–97.
10. Borovikova LV, Ivanova S, Zhang M, Yang H, Botchkina GI, Watkins LR, et al. Vagus nerve stimulation attenuates the systemic inflammatory response to endotoxin. Nature 2000;405:458–62.
11. Huston JM, Gallowitsch-Puerta M, Ochani M, Ochani K, Yuan R, Rosas-Ballina M, et al. Transcutaneous vagus nerve stimulation reduces serum high mobility group box 1 levels and improves survival in murine sepsis. Crit Care Med 2007;35:2762–8.
12. Uemura K, Li M, Tsutsumi T, Yamazaki T, Kawada T, Kamiya A, et al. Efferent vagal nerve stimulation induces tissue inhibitor of metalloproteinase-1 in myocardial ischemia-reperfusion injury in rabbit. Am J Physiol Heart Circ Physiol 2007;293:H2254–61.
13. LaCroix C, Freeling J, Giles A, Wess J, Li YF. Deficiency of M2 muscarinic acetylcholine receptors increases susceptibility of ventricular function to chronic adrenergic stress. Am J Physiol Heart Circ Physiol 2008;294:H810–20.
14. Hasdemir C, Scherlag BJ, Yamanashi WS, Lazzara R, Jackman WM. Endovascular stimulation of autonomic neural elements in the superior vena cava using a flexible loop catheter. Jpn Heart J 2003;44: 417–27.
15. Dewald O, Ren G, Duerr GD, Zoerlein M, Klemm C, Gersch C, et al. Of mice and dogs: species-specific differences in the inflammatory response following myocardial infarction. Am J Pathol 2004;164:665–77.
16. Gwechenberger M, Mendoza LH, Youker KA, Frangogiannis NG, Smith CW, Michael LH, et al. Cardiac myocytes produce interleukin-6 in culture and in viable border zone of reperfused infarctions. Circulation 1999;99:546–51.
17. Klotz S, Foronjy RF, Dickstein ML, Gu A, Garrelds IM, Danser AH, et al. Mechanical unloading during left ventricular assist device support increases left ventricular collagen cross-linking and myocardial stiffness. Circulation 2005;112:364–74.
18. Villarreal FJ, Griffin M, Omens J, Dillmann W, Nguyen J, Covell J. Early short-term treatment with doxycycline modulates postinfarction left ventricular remodeling. Circulation 2003;108:1487–92.
19. Newman KM, Ogata Y, Malon AM, Irizarry E, Gandhi RH, Nagase H, et al. Identification of matrix metalloproteinases 3 (stromelysin-1) and 9 (gelatinase B) in abdominal aortic aneurysm. Arterioscler Thromb 1994;14:1315–20.
20. Emens L, Rouy D, Velot E, Devaux Y, Wagner DR. Adenosine inhibits matrix metalloproteinase-9 secretion by neutrophils: implication of A2a receptor and cAMP/PKA/Ca2+ pathway. Circ Res 2006;99: 590–7.
21. Ørn S, Manhenke C, Anand IS, Squire I, Nagel E, Edvardsen T, et al. Effect of left ventricular scar size, location, and transmurality on left ventricular remodeling with healed myocardial infarction. Am J Cardiol 2007;99:1109–14.
22. Kakinuma Y, Ando M, Kuwabara M, Katare RG, Okudela K, Kobayashi M, et al. Acetylcholine from vagal stimulation protects cardiomyocytes against ischemia and hypoxia involving additive nonhypoxic induction of HIF-1alpha. FEBS Lett 2005;579:2111–8.
23. Frangogiannis NG, Lindsey ML, Michael LH, Youker KA, Bressler RB, Mendoza LH, et al. Resident cardiac mast cells degranulate and release preformed TNF-alpha, initiating the cytokine cascade in experimental canine myocardial ischemia/reperfusion. Circulation 1998;98:699–710.
24. Kindt F, Wiegand S, Niemeier V, Kupfer J, Löser C, Nilles M, et al. Reduced expression of nicotinic alpha subunits 3, 7, 9 and 10 in lesional and nonlesional atopic dermatitis skin but enhanced expression of alpha subunits 3 and 5 in mast cells. Br J Dermatol 2008;159: 847–57.
25. Smart N, Mojet MH, Latchman DS, Marber MS, Duchen MR, Heads RJ. IL-6 induces PI 3-kinase and nitric oxide-dependent protection and preserves mitochondrial function in cardiomyocytes. Cardiovasc Res 2006;69:164–77.
26. Rakhit RD, Seiler C, Wustmann K, Zbinden S, Windecker S, Meier B, et al. Tumour necrosis factor-alpha and interleukin-6 release during primary percutaneous coronary intervention for acute myocardial infarction is related to coronary collateral flow. Coron Artery Dis 2005;16:147–52.
27. Buck JD, Warltier DC, Hardman HF, Gross GJ. Effects of sotalol and vagal stimulation on ischemic myocardial blood flow distribution in the canine heart. J Pharmacol Exp Ther 1981;216:347–51.
28. Ørn S, Manhenke C, Ueland T, Damås JK, Mollnes TE, Edvardsen T, et al. C-reactive protein, infarct size, microvascular obstruction, and left-ventricular remodelling following acute myocardial infarction. Eur Heart J 2009;30:1180–6.
29. Nijmeijer R, Lagrand WK, Lubbers YT, Visser CA, Meijer CJ, Niessen HW, et al. C-reactive protein activates complement in infarcted human myocardium. Am J Pathol 2003;163:269–75.
30. Sukhija R, Fahdi I, Garza L, Fink L, Scott M, Aude W, et al. Inflammatory markers, angiographic severity of coronary artery disease, and patient outcome. Am J Cardiol 2007;99:879–84.
31. Blankenberg S, McQueen MJ, Smieja M, Pogue J, Balion C, Lonn E, et al. Comparative impact of multiple biomarkers and N-Terminal pro-brain natriuretic peptide in the context of conventional risk factors for the prediction of recurrent cardiovascular events in the Heart Outcomes Prevention Evaluation (HOPE) Study. Circulation 2006;114: 201–8.
32. Kelly D, Cockerill G, Ng LL, Thompson M, Khan S, Samani NJ, et al. Plasma matrix metalloproteinase-9 and left ventricular remodelling after acute myocardial infarction in man: a prospective cohort study. Eur Heart J 2007;28:711–8.
33. Lindsey ML, Gannon J, Aikawa M, Schoen FJ, Rabkin E, Lopresti-Morrow L, et al. Selective matrix metalloproteinase inhibition reduces left ventricular remodeling but does not inhibit angiogenesis after myocardial infarction. Circulation 2002;105:753–8.
34. Spinale FG, Escobar GP, Hendrick JW, Clark LL, Camens SS, Mingoia JP, et al. Chronic matrix metalloproteinase inhibition following myocardial infarction in mice: differential effects on short and long-term survival. J Pharmacol Exp Ther 2006;318:966–73.
35. van den Borne SW, Cleutjens JP, Hanemaaijer R, Creemers EE, Smits JF, Daemen MJ, et al. Increased matrix metalloproteinase-8 and -9 activity in patients with infarct rupture after myocardial infarction. Cardiovasc Pathol 2009;18:37–43.
36. Lindsey ML, Escobar GP, Mukherjee R, Goshorn DK, Sheats NJ, Bruce JA, et al. Matrix metalloproteinase-7 affects connexin-43 levels, electrical conduction, and survival after myocardial infarction. Circulation 2006;113:2919–28.
37. Li D, Zhao L, Liu M, Du X, Ding W, Zhang J, et al. Kinetics of tumor necrosis factor alpha in plasma and the cardioprotective effect of a monoclonal antibody to tumor necrosis factor alpha in acute myocardial infarction. Am Heart J 1999;137:1145–52.
38. Landmesser U, Wollert KC, Drexler H. Potential novel pharmacological therapies for myocardial remodelling. Cardiovasc Res 2009;81: 519–27.
39. Liu C, Shen FM, Le YY, Kong Y, Liu X, Cai GJ, Chen AF, Su DF. Antishock effect of anisodamine involves a novel pathway for activating alpha7 nicotinic acetylcholine receptor. Crit Care Med 2009;37: 634–41.
40. Nossuli TO, Lakshminarayanan V, Baumgarten G, Taffet GE, Ballantyne CM, Michael LH, et al. A chronic mouse model of myocardial ischemia-reperfusion: essential in cytokine studies. Am J Physiol Heart Circ Physiol 2000;278:H1049–55.

Acta Biomaterialia 6 (2010) 1925–1930

Contents lists available at ScienceDirect

Acta Biomaterialia

journal homepage: www.elsevier.com/locate/actabiomat

Stable modification of poly(lactic acid) surface with neurite outgrowth-promoting peptides via hydrophobic collagen-like sequence

Sachiro Kakinoki, Tetsuji Yamaoka *

Department of Biomedical Engineering, National Cardiovascular Center Research Institute, 5-7-1 Fujishirodai, Suita, Osaka 565-8565, Japan
JST, CREST, 5 Sanbancho, Chiyoda-ku, Tokyo 102-0075, Japan

ARTICLE INFO

Article history:
Received 30 July 2009
Received in revised form 11 November 2009
Accepted 1 December 2009
Available online 5 December 2009

Keywords:
Surface modification
PLA scaffold
Peptide adsorption
Hydrophobic interaction
Neurite outgrowth-promoting peptide

ABSTRACT

Surface modification of poly(DL-lactic acid) (PLA) scaffolds has been performed using a biofunctional small peptide composed of collagen-like repetitive sequence and laminin-derived sequence (AG73-G_3-$(PPG)_5$) via hydrophobic interaction. The results of surface analysis suggest that AG73-G_3-$(PPG)_5$ can be stably adsorbed onto PLA films via hydrophobic interaction at the $(PPG)_5$ region, and form an extracellular matrix-like layer composed of both structural and biosignalling sequences. In addition, neurite outgrowth of PC12 cells was observed on the AG73-G_3-$(PPG)_5$-adsorbed PLA film. These results indicate that AG73-G_3-$(PPG)_5$ very effectively enhances neurite outgrowth activity on PLA films. The hydrophobic adsorption of collagen-like peptide bound to biosignalling molecules may be widely applied as a surface modifier of PLA films for tissue engineering.

© 2009 Acta Materialia Inc. Published by Elsevier Ltd. All rights reserved.

1. Introduction

Tissue engineering has been proposed as an approach to replace damaged, injured or missing tissue with biologically compatible substrate combining cells or biosignalling molecules and scaffolds [1,2]. Scaffolds assume the role of a temporary extracellular matrix (ECM) where biodegradability and biocompatibility are essential for tissue regeneration. Furthermore, biodegradable scaffolds should be designed not to obstruct tissue regeneration via cell-induced natural healing. The cellular responses to the scaffold surfaces determine whether tissue regeneration will be promoted or obstructed. Therefore, it is very important to control the biological property of the scaffold surfaces [3].

Poly(lactic acid) (PLA) is widely used for biodegradable scaffolds as it possesses a number of suitable characteristics for this role. PLA can be hydrolytically degraded into lactic acid; this degradation requires only water, and the final product can immediately be metabolized in vivo [4]. Moreover, PLA material exhibits excellent shaping and molding properties because of its mechanical versatility. However, insufficient interaction between PLA materials and cells leading to in vivo foreign-body reactions is a major problem because the required biological activities are not inherent in PLA. PLA lacks functional groups and so cannot be easily modified with bioactive molecules. Therefore, many investigators have attempted to impart functional groups to PLA in order to enhance its biological activity by using copolymerization or chemical grafting with other polymers [5], plasma treatment [6], chemical modification [7] and physical adsorption. In previous studies, we reported on the preparation of poly(lactic-co-malic acid)-conjugated Arg-Gly-Asp (RGD) tripeptide [8] and gelatin-immobilized PLA scaffold [9] in order to improve the cell attachment. However, because these techniques are prone to adverse chemical reactions, it is necessary to develop techniques that are simpler and offer better biocompatibility. Physical adsorption, which is driven by electrostatic, hydrophobic and specific interactions, has been noted as a simpler surface modification technique of PLA scaffolds [10–12].

In the current work, neurite outgrowth-promoting peptides, consisting of laminin-derived sequence and collagen-like sequence, were designed as surface modifiers of PLA films via hydrophobic adsorption. PLA is preferred as a base material for a nerve regeneration conduit because of its excellent shaping and molding properties [13]. However, PLA does not inherently cater to any nerve regeneration activity. If biologically modified PLA-based artificial nerve can promote nerve regeneration, it might be possible to avoid donor site defects in autologous nerve transplantation. It was reported that laminin-derived sequence AG73 supports neurite outgrowth [14], and therefore was selected as a nerve-regenerating peptide.

On the other hand, it is well known that collagen is a predominant component of ECM [15,16]. The major part of collagen

* Corresponding author. Address: Department of Biomedical Engineering, National Cardiovascular Center Research Institute, 5-7-1 Fujishirodai, Suita, Osaka 565-8565, Japan. Tel.: +81 6 6833 5012x2637; fax: +81 6 6835 5476.
E-mail address: yamtet@ri.ncvc.go.jp (T. Yamaoka).

1742-7061/$ - see front matter © 2009 Acta Materialia Inc. Published by Elsevier Ltd. All rights reserved.
doi:10.1016/j.actbio.2009.12.001

consists of Xaa-Yaa-Gly repetitive sequences, where Xaa and Yaa positions are often occupied by Pro and 4(R)-hydroxyproline (Hyp), respectively, and forms the hydrophobic polyproline-II (PP-II) structure [17–20]. The collagen triple-helix structure is composed of three PP-II chains, and collagen-like peptides (CLPs) such as $(Pro\text{-}Pro\text{-}Gly)_n$ are also able to form a triple-helix structure [21–23]; therefore, CLP is expected to be adsorbed by PLA films via hydrophobic interaction. Animal-derived collagen has also been intensively investigated as a conduit for nerve regeneration because of its high bioactivity [24]. However, animal-derived collagens possess high antigenicity in vivo because of the unnecessary biosignal sequences and enzymatically digested fragments [25]. CLP, which is the repetitive sequence at a structural region of collagen without any enzyme-digestible sequence, is anticipated to be of low immunogenicity.

Here, we are reporting on a neurite outgrowth-promoting peptide composed of AG73 and CLP (AG73-G_3-$(PPG)_5$) as a surface modifier of PLA films for tissue engineering. Conformation of AG73-G_3-$(PPG)_5$ was studied by circular dichroism (CD) spectroscopy. The surface characteristics of AG73-G_3-$(PPG)_5$-adsorbed PLA film were investigated by water contact angle measurement and X-ray photoelectron spectroscopy (XPS). PC12 cells were primed with nerve growth factor (NGF) and cultured on the AG73-G_3-$(PPG)_5$-adsorbed PLA films, and the neurite outgrowth activity was then quantified.

2. Materials and methods

2.1. Materials

$(PPG)_{10}$, AG73 (RKRLQVQLSIRT) and AG73-G_3-$(PPG)_5$ were commercially synthesized by SCRUM, Inc. (Tokyo, Japan). PLA (Mw 130,000) was obtained from Mitsui Chemicals, Inc. (Tokyo, Japan). Progesterone, sodium selenite (N_2SeO_3) and transferrin were purchased from Nacalai Tesque, Inc. (Kyoto, Japan). NGF and horse serum (HS) were obtained from Sigma–Aldrich, Inc. (St. Louis, MO, USA). Insulin, advanced DMEM/F12 and penicillin–streptomycin were purchased from Invitrogen Corporation (Carlsbad, CA, USA). Fetal bovine serum (FBS) was obtained from MP Biomedicals, Inc. (Solon, OH, USA).

2.2. Methods

2.2.1. Circular dichroism

CD spectra were measured by a J-720 spectropolarimeter (Jasco Co., Tokyo, Japan) with a standard analysis program. The temperature was controlled using a recirculating waterbath and spectra was recorded with a 0.1 cm path length cell, using a scanning speed 10 nm min^{-1}, with a 1.0 nm spectral bandwidth, over the wavelength range from 190 to 250 nm. Peptides were dissolved with water at 0.25 mM. Data are represented in molar elipticities ($[\theta]$ deg cm^2 $dmol^{-1}$).

2.2.2. Peptide adsorption on PLA films

PLA films (diameter $\varphi = 6.0$ mm; $t = 0.5$ mm) were prepared with a hot shrinking machine at 180 °C and sterilized by UV irradiation. Three peptides, $(PPG)_{10}$, AG73, and AG73-G_3-$(PPG)_5$, were dissolved in sterilized water at 10 μM, and then 1 ml of each peptide solution was poured onto a PLA film in a 24-well cell culture plate. Peptide solutions were dried for 24 h. In order to get rid of any excessively adsorbed peptide, the PLA films were washed with 1 ml of sterilized H_2O or 1.0 M NaCl aqueous solution twice for 30 min, and then the films were washed with 1 ml of sterilized H_2O again and dried in vacuo.

2.2.3. Water contact angle

The contact angle with distilled water was measured by using a contact-angle meter (CA-X; Kyowa Interface Science Co., Ltd., Saitama, Japan). Images of the water spreading on the sample were recorded by a camera and then analyzed. Three samples were measured for each group.

2.2.4. X-ray photoelectron spectroscopy

The surface composition of peptide-adsorbed PLA films was determined using an ESCA-3400 (Shimadzu Co., Kyoto, Japan). The X-ray source was a monochromatic Mg K_α X-ray from a rotating anode. Survey scans were measured from 0 to 1200 eV. Peak positions and areas were analyzed and ratios for C1s, N1s and O1s were calculated by using software provided by the manufacturer.

2.3. Cell culture

Rat adrenal pheochromocytoma PC12 cells (RIKEN BioResource Center, Ibaraki, Japan) were maintained in DMEM supplemented with 100 U ml^{-1} penicillin, 100 μg ml^{-1} streptomycin, 10% FBS and 7.5% HS. PC12 cells were cultured in poly-D-Lys coated cell-culture dishes (BD, NJ, USA) and maintained at 37 °C in an atmosphere of 5% CO_2 and 95% air.

2.4. Neurite outgrowth assay

The neurite outgrowth assay was performed by using PC12 cells as the model of neural stem cells [26]. PC12 cells were primed with 100 ng ml^{-1} NGF for 24 h on polystyrene cell-culture dishes. The cells were then collected by agitation and placed in the culture medium for 30 min at 37 °C in an atmosphere of 5% CO_2 and 95% air. The cells were washed and resuspended with advanced DMEM/F12 containing 5 μg ml^{-1} insulin, 100 ng ml^{-1} NGF, 20 nM progesterone, 30 nM Na_2SeO_3 and 100 mg ml^{-1} transferrin. The cells were then seeded on peptide-adsorbed PLA films at a seeding density of 2.0×10^4 cells $film^{-1}$ in 24-well cell culture plates, and incubated at 37 °C for 24 h. PC12 cells on peptide-adsorbed PLA films were fixed with 10% formalin and stained by 4% crystal violet/methanol solution, and then the number of PC cells with or without neurites was determined in order to evaluate the neurite outgrowth activity as described elsewhere [27,28]. The lengths of neurites were measured using software (Image J; National Institute of Mental Health, MD, USA) [29]. Cells with neurites longer than 50 μm and those with neurites shorter than 50 μm were counted separately.

3. Results and discussion

3.1. Secondary structure of peptides

The CD spectra of $(PPG)_{10}$, AG73 and AG73-G_3-$(PPG)_5$ are shown in Fig. 1. The CD spectrum of $(PPG)_{10}$ in water at 37 °C exhibited a strong negative band at 209 nm and a positive band at 229 nm, which are known as typical patterns of collagen triple-helix and PP-II structure [20,30]. Although the CD spectrum of PP-II is similar to that of collagen triple-helix, the transition temperature of $(PPG)_{10}$ is reported to be about 28 °C in water [31]. Therefore, this CD spectrum indicates that $(PPG)_{10}$ forms the PP-II structure. The CD spectrum of AG73 showed a strong negative band at 199 nm, assigned as a random-coil structure. In the case of AG73-G_3-$(PPG)_5$, the CD spectrum indicated an intermediate pattern between $(PPG)_{10}$ and AG73. This means that a negative band was blue-shifted and a positive band at 229 nm was decreased in comparison with $(PPG)_{10}$. In addition, all CD spectra have an isosbestic

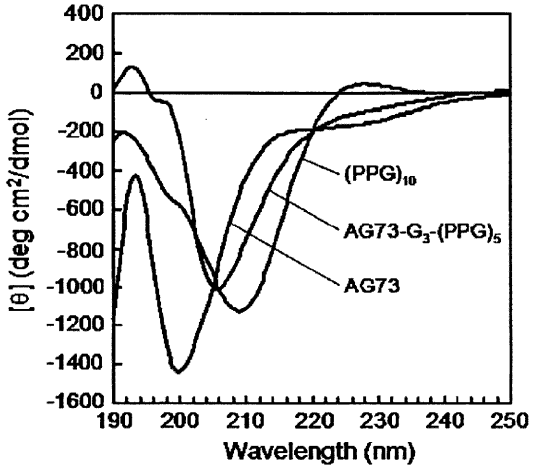

Fig. 1. Circular dichroism spectra of $(PPG)_{10}$, AG73 and AG73-G_3-$(PPG)_5$ in water.

point at 220 nm. The results suggest that the CLP region of AG73-G_3-$(PPG)_5$ also forms the PP-II structure. It is well known that the PP-II structure is the predominant secondary structure in collagen triple-helix. In addition, the PP-II structure of $(PPG)_n$ repetitive sequence exposes hydrophobic five-membered rings of Pro residues. Therefore, it is inferred that $(PPG)_n$ is adsorbed onto PLA films via hydrophobic interaction.

3.2. Surface characterization of peptide-adsorbed PLA films

To compare the hydrophilicity of the peptide-adsorbed PLA film surfaces, the water contact angle was measured (Table 1). The water contact angle of non-adsorbed PLA films was 79.1 ± 1.2°, which indicates a hydrophobic surface. After adsorption of $(PPG)_{10}$, AG73 and AG73-G_3-$(PPG)_5$, the water contact angle changed to 70.1 ± 3.9°, 31.2 ± 2.1° and 55.6 ± 1.9°, respectively. The water contact angle drastically decreased with AG73 and AG73-G_3-$(PPG)_5$ adsorption, but with $(PPG)_{10}$ adsorption the decrease was considerably less. It seems that the surface wettability of peptide-adsorbed PLA films corresponded to the hydrophilicity of the peptides, i.e. $(PPG)_{10}$ is more hydrophobic than AG73 and AG73-G_3-$(PPG)_5$. Safinia et al. reported that the PLA film surface shows a negative ζ-potential at physiological pH [32] because of a carboxyl group at the terminal of the PLA molecule. Therefore, the results suggest that these peptides are adsorbed onto PLA film via hydrophobic or electrostatic interactions.

The XPS N1s spectrum is shown in Fig. 2. The XPS spectra of $(PPG)_{10}$-, AG73- and AG73-G_3-$(PPG)_5$-adsorbed PLA films exhibited a N1s peak corresponding to amino acids. In order to compare the adsorbed peptide ratio on PLA films, the elemental ratios are summarized in Table 2. N1s was not detected clearly because PLA itself does not contain nitrogen. The N1s/C1s ratios were 0.07, 0.09 and 0.18, and the N1s/O1s ratios were 0.03, 0.04 and 0.09. The N1s/C1s and N1s/O1s ratios were increased with peptide adsorption; in particular, the highest values were shown for AG73-G_3-$(PPG)_5$. The AG73-G_3-$(PPG)_5$ might be adsorbed at high density via hydrophobic interaction between $(PPG)_5$ region and PLA. The reason for the decrease in water contact angle of AG73-G_3-$(PPG)_5$-adsorbed PLA film (Table 1) is that the hydrophilic AG73 region in AG73-G_3-$(PPG)_5$ was partially exposed to solution. Ji et al. also indicated that the poly(ethylene oxide–propylene oxide–ethylene oxide) amphiphilic triblock copolymer bearing RGD tripeptides adsorbed onto PLA films through hydrophobic interaction, and its hydrophilic regions were exposed to solution phase [11]. As a result, the AG73-G_3-$(PPG)_5$ adsorbs via hydrophobic interaction and constructs an ECM-like layer on the PLA film surface.

Table 1
Water contact angle of peptide-adsorbed PLA films.

	CA (°)
Non-adsorbed	79.1 ± 1.2
$(PPG)_{10}$	70.1 ± 3.9
AG73	31.2 ± 2.1
AG73-G_3-$(PPG)_5$	55.6 ± 1.9

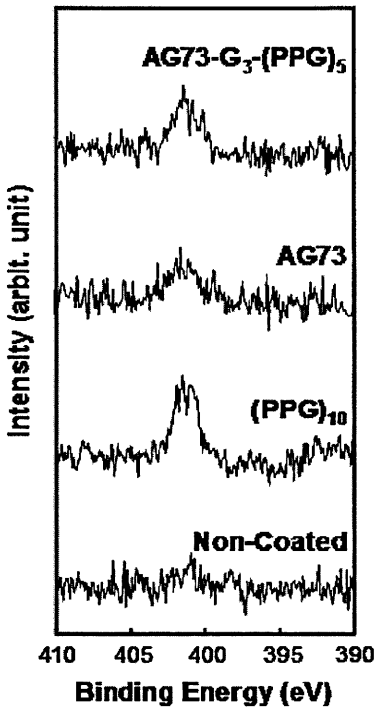

Fig. 2. XPS spectra of the N1s region of peptide-adsorbed PLA films.

Table 2
Elemental ratio of nitrogen to carbon (N1s/C1s) or oxygen (N1s/O1s) measured by XPS.

	PLA	$(PPG)_{10}$	AG73	AG73-G_3-$(PPG)_5$
N1s/C1s	0.01	0.07	0.09	0.18
N1s/O1s	0.00	0.03	0.04	0.09

3.3. Neurite outgrowth activity of peptide-adsorbed PLA films

The morphology of PC12 cells on peptide-adsorbed PLA films is shown in Fig. 3a, and the number of adhered PC12 cells with or without neurites is summarized in Fig. 3b. On the naked and $(PPG)_{10}$-adsorbed PLA films, PC12 cells (~230 cells mm^{-2}) did not adhere well enough, and so neurite outgrowth could not be found. This indicates that $(PPG)_n$ itself does not support bioactivity for cell adhesion or neurite outgrowth. Meanwhile, on AG73- and AG73-G_3-$(PPG)_5$-adsorbed PLA films, the adhesion of PC12 cells was improved to more than 300 cells mm^{-2}. Neurite outgrowth also occurred, i.e. the number of PC12 cells with neurites was more than 75% on both AG73- and AG73-G_3-$(PPG)_5$-adsorbed PLA films. In contrast, the mechanisms of adsorption of these films must be different from each other since the physicochemical properties of AG73 and AG73-G_3-$(PPG)_5$ are quite dissimilar. As mentioned above, they are considered to be adsorbed onto PLA films via

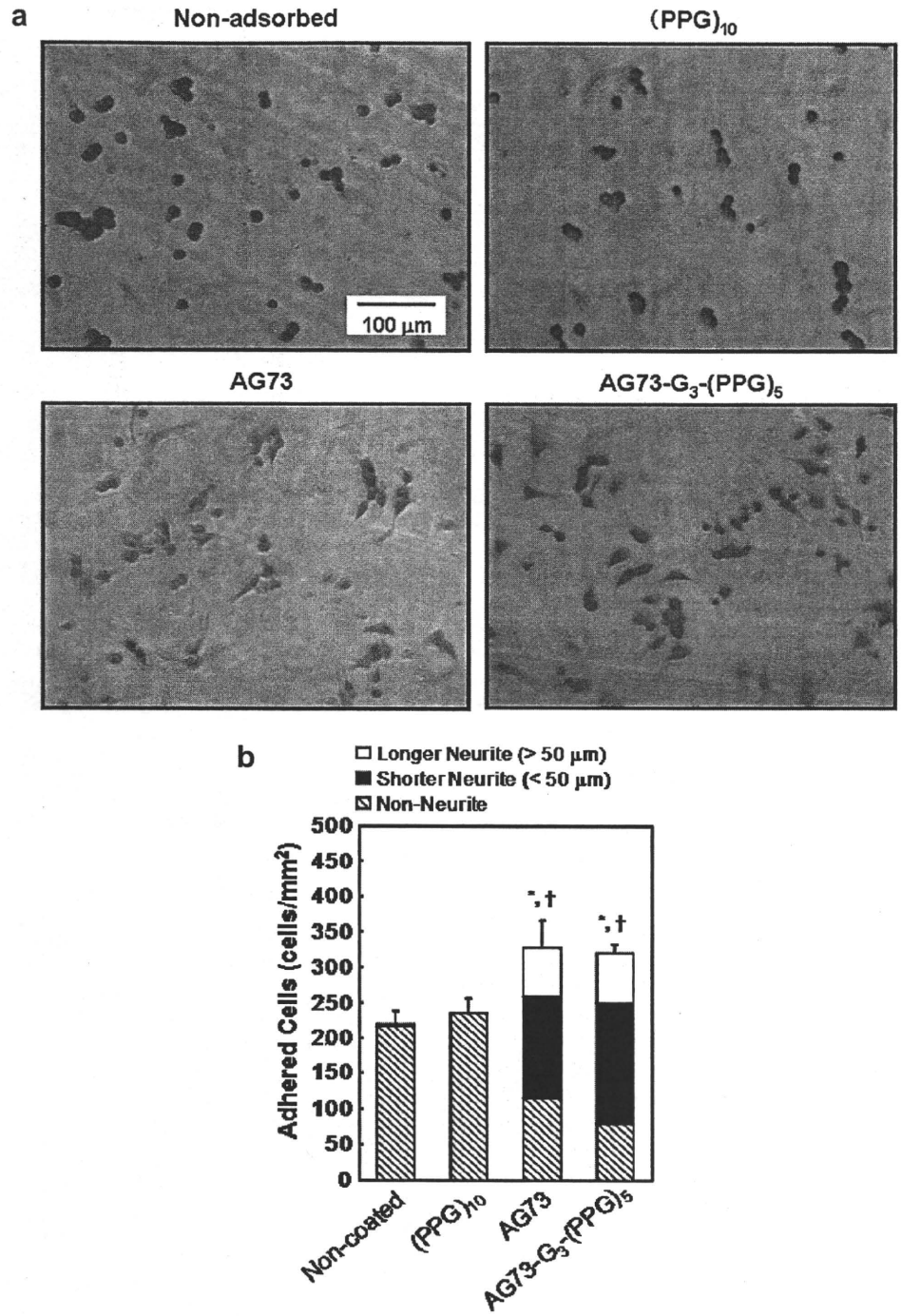

Fig. 3. Neurite outgrowth activity of PC12 cells on peptide-adsorbed PLA films. (a) Morphology of PC12 cells on peptide-adsorbed PLA films after 24 h. (b) The number of adhered PC12 cells on peptide-adsorbed PLA films with and without neurites. $^{*}P < 0.05$ when AG73 and AG73-G_3-$(PPG)_5$ groups compared with non-coated group; $^{\dagger}P < 0.05$ when AG73 and AG73-G_3-$(PPG)_5$ groups compared with $(PPG)_{10}$ group.

electrostatic and hydrophobic interactions, respectively. It is anticipated that under physiological conditions, adsorption of AG73-G_3-$(PPG)_5$ is more stable than that of AG73.

In order to evaluate the stability of the adsorbed AG73-G_3-$(PPG)_5$, neurite outgrowth assay was performed on AG73 and AG73-G_3-$(PPG)_5$-adsorbed PLA films after washing with 1.0 M NaCl aqueous solution (Fig. 4). In the case of AG73-adsorbed PLA films, the number of adhered PC12 cells is decreased to below 60% by 1.0 M NaCl washing, but the ratio of PC12 cells with neurites remains unchanged. After 1.0 M NaCl washing, the water contact angles of $(PPG)_{10}$-, AG73- and AG73-G_3-$(PPG)_5$-adsorbed PLA films changed from $70.1 \pm 3.9°$, $31.2 \pm 2.1°$ and $55.6 \pm 1.9°$ to $70.3 \pm 1.5°$, $60.0 \pm 1.3°$ and $54.6 \pm 4.2°$, respectively. That is, the water contact angle of the AG73-adsorbed PLA films was drastically increased by 1.0 M NaCl washing, but that of AG73-G_3-$(PPG)_5$-adsorbed films was changed a little. These results indicated that adsorbed AG73 seemed to be partially removed by 1.0 M NaCl washing, and the remaining AG73 expressed neurite outgrowth-promoting activity, because AG73 was mainly adsorbed via electrostatic interaction. Meanwhile, the number of adhered PC12 cells was not changed and neurite outgrowth was also found on AG73-G_3-$(PPG)_5$-adsorbed PLA films after washing with H_2O or 1.0 M

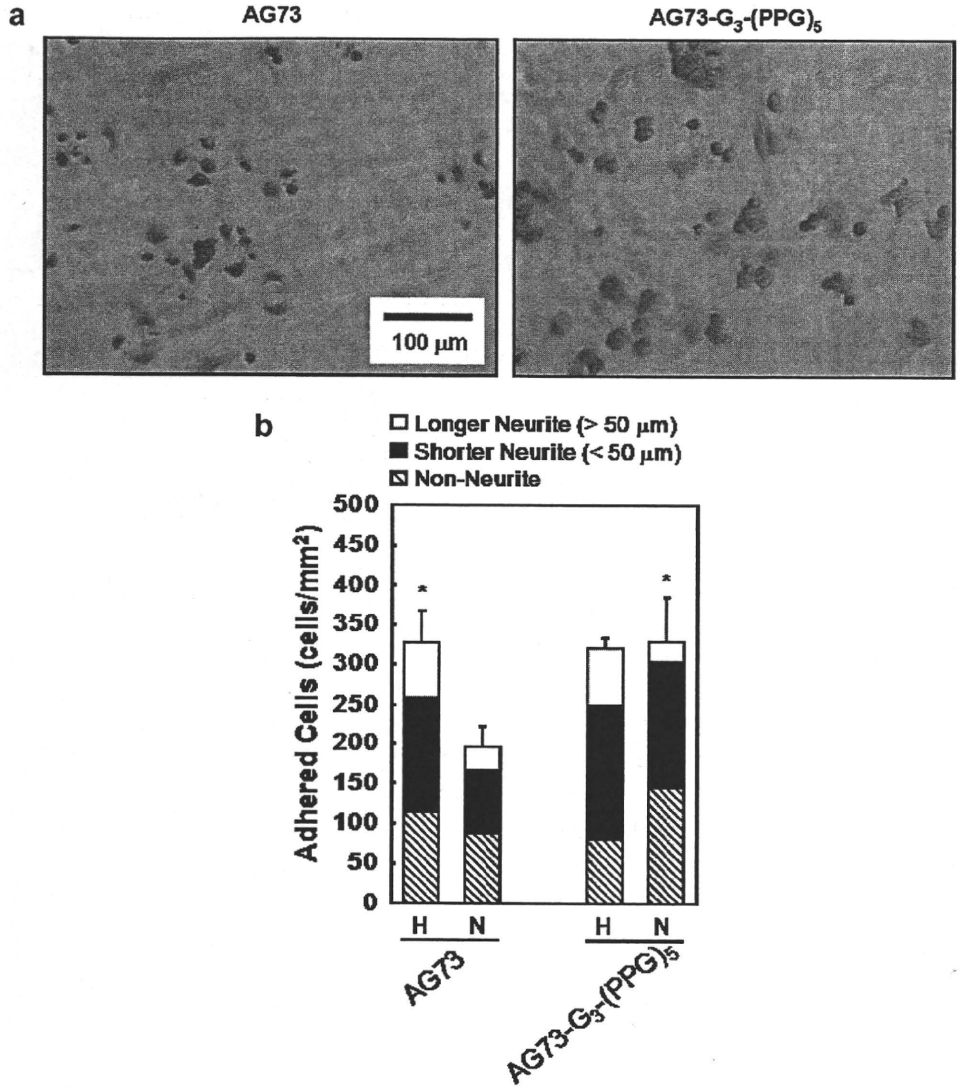

Fig. 4. Neurite outgrowth activity of PC12 cells on AG73- and AG73-G_3-$(PPG)_5$-adsorbed PLA films after washing with H_2O (H) or 1.0 M NaCl aq. (N). (a) Morphology of PC12 cells after 24 h. PLA films were modified with peptides, washed with 1.0 M NaCl and subjected to PC12 cell culture. (b) The number of adhered PC12 cells on peptide adsorbed PLA films with and without neurites. * $P < 0.05$ when AG73 (H) and AG73-G_3-$(PPG)_5$ (N) groups are compared with AG73 (N) group.

NaCl. Hydrophobic interaction generally becomes stronger in the presence of salts because of the dehydration of the surface and adsorbents. The ratio of PC12 cells with neurites was slightly decreased by 1.0 M NaCl washing, because a partial AG73-G_3-$(PPG)_5$ was adsorbed by PLA films via electrostatic interaction. As result, it is proposed that PLA films adsorb AG73-G_3-$(PPG)_5$ mainly by hydrophobic interaction, and an ECM-like layer composed of structural protein and biosignalling sequences is formed. It is known that animal-derived collagen, like laminin, also promotes neurite outgrowth, because it is a fusion protein that combines a structural protein with many biosignal sequences [33]. Neurite outgrowth is mainly promoted by biosignal sequences in collagen, and it must be supported by the structural properties of these sequences. We believe that the structural properties of the ECM-like layer composed of AG73-G_3-$(PPG)_5$ creates a synergy with AG73 biosignalling for promoting neurite outgrowth.

4. Conclusion

Hydrophobic peptide-based interfacial adsorption onto PLA films and film stability have been characterized. Collagen-laminin mimics peptide AG73-G_3-$(PPG)_5$ and forms the hydrophobic PP-II structure in the $(PPG)_5$ region. Therefore, AG73-G_3-$(PPG)_5$ was capable of exhibiting stable adsorption onto PLA films via hydrophobic interaction, resulting in promotion of neurite outgrowth of PC12 cells. Furthermore, AG73-G_3-$(PPG)_5$, which is composed of biosignalling and structural protein-like sequences, forms an ECM-like layer on PLA films. It has recently been noted that the mechanical and morphological properties of ECMs are important for controlling stem cell differentiation [34]. The hydrophobic adsorption of collagen-like peptide is expected to serve as a surface modification technique of PLA films for controlling the biological properties of cells.

Acknowledgements

The authors thank Dr. Aasako Yamayoshi and Prof. Akira Murakami at the Kyoto Institute of Technology for assistance with the circular dichroism measurements. This work was partly supported by a Grant-in-Aid for Scientific Research (KAKENHI) promoted by the Ministry of Education, Culture, Sports and Technology, Japan.

Appendix A. Figures with essential color discrimination

Certain figures in this article, particularly Figs. 3 and 4, are difficult to interpret in black and white. The full color images can be found in the on-line version, at doi: 10.1016/j.actbio.2009.12.001.

References

[1] Lanza R, Langer R, Vacanti J, editors. Principles of tissue engineering. Amsterdam and Boston, MA: Elsevier/Academic Press; 2007.
[2] Tabata Y. Biomaterial technology for tissue engineering applications. J R Soc Interface 2009;6:S311–24.
[3] Ma Z, Mao Z, Gao C. Surface modification and property analysis of biomedical polymers used for tissue engineering. Colloids Surf B Biointerfaces 2007;60:137–57.
[4] Gupta B, Revagade N, Hilborn J. Poly(lactic acid) fiber: an overview. Prog Polym Sci 2007;32:455–82.
[5] Jiao YP, Cui FZ. Surface modification of polyester biomaterials for tissue engineering. Biomed Mater 2007;2:R24–37.
[6] Khorasani MT, Mirzadeh H, Irani S. Plasma surface modification of poly(L-lactic acid) and poly(lactic-co-glycolic acid) films for improvement of nerve cells adhesion. Rad Phys Chem 2008;77:280–7.
[7] Ma Z, Gao C, Ji J, Shen J. Protein immobilization on the surface of poly-L-lactic acid films for improvement of cellular interactions. Eur Polym J 2002;38:2279–84.
[8] Yamaoka T, Hotta Y, Kobayashi K, Kimura Y. Synthesis and properties of malic acid-containing functional polymers. Int J Biol Macromol 1999;25:265–71.
[9] Yamaoka T, Takebe Y, Kimura Y. Surface modification of poly(L-lactic acid) film with bioactive materials by a novel direct alkaline treatment process. Kobunshi Ronbunshu 1998;55:328–33.
[10] Zhu H, Ji J, Barbosa MA, Shen J. Protein electrostatic self-assembly on poly(DL-lactide) scaffold to promote osteoblast growth. J Biomed Mater Res B Appl Biomater 2004;71:159–65.
[11] Ji J, Zhu H, Shen J. Surface tailoring of poy(DL-lactic acid) by ligand-tethered amphiphilic polymer for promoting chondrocyte attachment and growth. Biomaterials 2004;25:1859–67.
[12] Matsuno H, Sekine J, Yajima H, Serizawa T. Biological selection of peptides for poly(L-lactide) substrates. Langmuir 2008;24:6399–403.
[13] Oh SH, Kim JH, Song KS, Jeon BH, Yoon JH, Seo TB, et al. Peripheral nerve regeneration within an asymmetrically porous PLGA/Pluronic F127 nerve guide conduit. Biomaterials 2008;29:1601–9.
[14] Weeks BS, Nomizu M, Ramachandran RS, Yamada Y, Kleinman HK. Laminin-1 and the RKRLQVQLSIRT laminin-1 α1 globular domain peptide stimulate matrix metalloproteinase secretion by PC12 cells. Exp Cell Res 1998;243:375–82.
[15] Koide T. Designed triple-helical peptides as tools for collagen biochemistry and matrix engineering. Philos Trans R Soc B 2007;362:1281–91.
[16] Abraham LC, Zuena E, Perez-Ramirez B, Kaplan DL. Guide to collagen characterization for biomaterial studies. J Biomed Mater Res B Appl Biomater 2008;87:264–85.
[17] Jenkins CL, Raines RT. Insights on the conformational stability of collagen. Nat Prod Rep 2002;19:49–59.
[18] Engel J, Bachinger HP. Structure, stability and folding of the collagen triple helix. Top Curr Chem 2005;247:7–33.
[19] Okuyama K. Revisiting the molecular structure of collagen. Connect Tissue Res 2008;49:299–310.
[20] Kakinoki S, Hirano Y, Oka M. On the stability of polyproline-I and II structures of proline oligopeptides. Polym Bull 2005;53:109–15.
[21] Kobayashi Y, Sakai R, Kaniuchi K, Isemura T. Physicochemical analysis of (Pro-Pro-Gly)$_n$ with defined molecular weight-temperature dependence of molecular weight in aqueous solution. Biopolymers 1970;9:415–25.
[22] Gough CA, Anderson RW, Bhatnagar RS. The role of bound water in the stability of the triple-helical conformation of (Pro-Pro-Gly)$_{10}$. J Biomol Struct Dyn 1998;15:1029–37.
[23] Stetefeld J, Frank S, Jenny M, Schulthess T, Kammerer RA, Boudko S, et al. Collagen stabilization at atomic level: crystal structure of designed (GlyProPro)$_{10}$ folden. Structure 2003;11:339–46.
[24] Inada Y, Morimoto S, Moroi K, Endo K, Nakamura T. Surgical relief of causalgia with an artificial nerve guide tube: successful surgical treatment of causalgia (Complex Regional Pain Syndrome Type II) by in situ tissue engineering with a polyglicolic acid-collagen tube. Pain 2005;117:251–8.
[25] Andair-Kirk TL, Senior RM. Fragments of extracellular matrix as a mediators of inflammation. Int J Biochem Cell Biol 2008;40:1101–10.
[26] Greene LA, Tischler AS. Establishment of a noradrenergic clonal line of rat adrenal pheochromocytoma cells which respond to nerve growth factor. Proc Natl Acad Sci USA 1976;73:2424–8.
[27] Mochizuki M, Kadoya Y, Wakabayashi Y, Kato K, Okazaki I, Yamada M, et al. Laminin-1 peptide-conjugated chitosan membranes as a novel approach for cell engineering. FASEB J 2003;17:875–7.
[28] Ichikawa N, Kasai S, Suzuki N, Nishi N, Oishi S, Fujii N, et al. Identification of neurite outgrowth active sites on the laminin α4 chain G domain. Biochemistry 2005;44:5755–62.
[29] Collins TJ. ImageJ for microscopy. Biotechniques 2007;43:S25–30.
[30] Jenness DD, Sprecher C, Curtis J. Circular dichroism of collagen, gelatin, and poly(proline) II in the vacuum ultraviolet. Biopolymers 1976;15:513–21.
[31] Khew ST, Tong YW. Characterization of triple-helical conformations and melting analyses of synthetic collagen-like peptides by reversed-phase HPLC. J Chromatogr B Analyt Technol Biomed Life Sci 2007;858:79–90.
[32] Safinia L, Datan N, Höhse M, Mantalaris A, Bismarck A. Towards a methodology for the effective surface modification of porous polymer scaffolds. Biomaterials 2005;26:7537–47.
[33] David CT, Leonard AF, Salvatore C. Identification of a cell-surface protein involved in PC12 cell-substratum adhesion and neurite outgrowth on laminin and collagen. J Neurosci 1989;9:3287–96.
[34] Hwang NS, Varghese S, Elisseeff J. Controlled differentiation of stem cells. Adv Drug Deliv Rev 2008;60:199–214.

Antibody-Immobilized Column for Quick Cell Separation Based on Cell Rolling

Atsushi Mahara and Tetsuji Yamaoka
Dept. of Biomedical Engineering, Advanced Medical Engineering Center, National Cardiovascular Center Research Institute, Suita, Osaka, Japan 565-8565

DOI 10.1002/btpr.354
Published online November 13, 2009 in Wiley InterScience (www.interscience.wiley.com).

Cell separation using methodological standards that ensure high purity is a very important step in cell transplantation for regenerative medicine and for stem cell research. A separation protocol using magnetic beads has been widely used for cell separation to isolate negative and positive cells. However, not only the surface marker pattern, e.g., negative or positive, but also the density of a cell depends on its developmental stage and differentiation ability. Rapid and label-free separation procedures based on surface marker density are the focus of our interest. In this study, we have successfully developed an antiCD34 antibody-immobilized cell-rolling column, that can separate cells depending on the CD34 density of the cell surfaces. Various conditions for the cell-rolling column were optimized including graft copolymerization, and adjustment of the column tilt angle, and medium flow rate. Using CD34-positive and -negative cell lines, the cell separation potential of the column was established. We observed a difference in the rolling velocities between CD34-positive and CD34-negative cells on antibody-immobilized microfluidic device. Cell separation was achieved by tilting the surface 20 degrees and the increasing medium flow. Surface marker characteristics of the isolated cells in each fraction were analyzed using a cell-sorting system, and it was found that populations containing high density of CD34 were eluted in the delayed fractions. These results demonstrate that cells with a given surface marker density can be continuously separated using the cell rolling column. © 2009 American Institute of Chemical Engineers *Biotechnol. Prog.*, 26: 441–447, 2010
Keywords: cell separation, cell rolling, surface marker, antibody, CD34

Introduction

Because they do not lead to immunoreactions, tissue-derived stem cells have been the subject of much interest as an autologous source of stem cells.[1,2] The first important step in regenerative medicine using stem cells is to isolate a sufficient quantity of high purity stem cells in the clinically permitted period.[3,4] However, the isolation of homogeneous stem cells harvested from the body along with other mature cells is complicated procedure. Generally, stem cells are purified on the basis of their density,[5] size,[6] adhesion properties,[7] or surface maker patterns.[8–12] Although density gradient centrifugation and separation by size-sieving are relatively simple and easy to perform, they are not specific for stem cells. The most popular method for isolating mesenchymal stem cells (MSCs) is separation of the adherent cells on a plastic culture dish.[7] However, this method of cell isolation is also unsatisfactory for obtaining highly homogeneous stem cell populations.[2,13]

In contrast, an antibody-based strategy is much more effective and specific. Various cell surface markers have been found to be useful in identifying every type of stem cell. Once identified, stem cells can be isolated using fluorescence-activated cell sorting (FACS) or magnetic-activated cell sorting (MACS) systems. These strategies have been useful for separating target cells with an identified cell surface marker from unpurified cell populations.[14] For clinical stem cell therapy in cardiac revascularization, unpurified bone marrow cells or purified bone marrow CD133+ cells were injected into the infarct area; in these treatments, improvement in both blood flow and left ventricular function were observed.[13] However, contamination with other cell populations has also been described as a potential hurdles for clinical cell-therapy.

The types of surface markers expressed, as well as the level of marker expression, depend on the differentiation or developmental stage.[15,16] For example, the CD34 expression level of hematopoietic stem cells continuously decreases with developmental stage.[17] In myogenic progenitor cells, the expression level of CD34 changes during its differentiation into a myotube.[16] Marker density is a critical factor for stem cell separation; however, the widely used MACS system is not sensitive to marker density. One effective approach to this problem is to use a gate to set fluorescence intensity in FACS. The FACS system requires a rapid flow for cell sorting, and this affects the viability of sorting cells. Moreover, the cells thus obtained are contaminated with fluorescence- or magnetic bead-modified antibodies, which must be subsequently removed for safety.

Additional Supporting Information may be found in the online version of this article

Correspondence concerning this article should be addressed to T. Yamaoka at yamtet@ri.ncvc.go.jp.

© 2009 American Institute of Chemical Engineers

As a solution to these problems, a novel cell separation system was designed based on the cell-rolling process that can separate cells with a given surface marker density. First reported by Andrian in 1991, the leukocyte-rolling mechanism has been defined as the temporal interaction between a leukocyte surface marker and endothelial cells on the blood vessel luminal surfaces.[18] Hammer et al. described the temporal interaction between the cell surface markers and the immobilized ligand in the flow media.[19] Detailed mechanisms of the rolling adhesion properties of cells have been reported by other groups.[20–25] This unique concept has also been applied in drug screening,[26] local delivery of therapeutics,[27] and studies of cell regulation.[22,28,29] Antibody-immobilized microfluidic devices and microfabricated-cell sorters have been developed for isolating target cells with an adequate surface marker using the positive/negative selection method.[30,31] Patterning surface of receptors has been used as a means of continuous separation of cells by cell rolling.[32] This mechanism effectively isolates large quantities of cells. However, the cells in this system are intermittently rolled on the surface, and cell rolling as well as tethering between the receptor-coated region and the unmodified region are induced by the pattern and its edge. This surface approach is also an effective method of cell separation by cell rolling.

In this study, we focused on whether CD34-positive cells could be finely separated based on the CD34 densities on their surface. The KG-1a cell line, which is CD34-positive, was used as the model, while the CD34-negative HL-60 cell line was used as the control. We developed a tubular column with a continuous surface for cell separation such that the anti-CD34 antibody was immobilized at a high density on the surface. Chemical immobilization of the antibody through poly(acrylic acid) graft polymerization prevents antibody contamination of the purified cells. The injected cells are rolled on the inner surface of the column due to the medium flow shear force, in a manner similar to that of the rolling adhesion process of a leukocyte in a blood vessel.[18] The cell suspensions of KG-1a or HL-60 were passed through the column, and the cell numbers and the surface marker pattern on the cells were evaluated in each elution fraction.

Materials and Methods

Culturing of KG-1a and HL-60 cells

CD34-positive KG-1a cells were grown in IMEM culture medium (Invitrogen, Carlsbad, CA) supplemented with 10% fetal bovine serum (FBS) (Sigma, St. Luis, MO), penicillin (100 U/mL), and streptomycin (100 μg/mL). CD34-negative HL-60 cells were grown in RPMI medium (Invitrogen, Carlsbad, CA) containing 20% FBS with antibiotics. The cell lines were cultured in a humidified atmosphere containing 5% CO_2 at 37°C.

Antibody-immobilized column

Polyethylene tubes with a 1-mm inner diameter were selected as the substrate for the cell-separation column. Graft polymerization of acrylic acid onto the column was conducted as follows. The tube was treated with ozone gas (ON-3-2, Nippon Ozone Co.Ltd., Tokyo, Japan) for 4 h, dipped in 0–30% acrylic acid/methanol solution, and incubated at 60°C. After 4 h, the tube was washed with water.[33,34] The graft polymerization was confirmed by toluidine blue staining. To immobilize the anti-CD34 antibody on the tube surface, the poly(acrylic acid)-grafted tube was activated using 1-ethyl-3-(3-dimethylaminopropyl) carbodiimide hydrochloride (WSC) under various conditions. Thereafter, the activated tube was filled with a 0.1 mg/mL solution of the monoclonal mouse anti-human CD34 class II antibody (Dako Ltd., Carpenteria, CA), and incubated at 37°C for 15 h. The tube was washed with PBS, treated with 1 mM 2-aminoethanol solution for 1 h and preserved at 4°C until experimental use. The antibody density on the luminal surface was evaluated using peroxidase conjugated anti-mouse IgG (whole molecule) antibody (Sigma, St. Luis, MO). Peroxidase activity was measured using the SMILON Peroxidase Detection Kit (Sumitomo Bakelite Co.,Ltd., Tokyo, Japan).

Separation of cells on the antibody-immobilized column

The antibody-immobilized column was connected using a syringe pump (Model:780120J; KD Scientific Inc., Hollistone, MA) through the unmodified tube. The length of the antibody-immobilized column and the unmodified tube was 100 mm, and the cell suspension was directly injected into the unmodified tube using a disposable syringe with a 27 G needle. The column was inclined against the ground, and the tilt angle was fixed by clamping. Cell separation was performed as follows. The KG-1a or HL-60 cell suspension (2×10^4 cells/50 μL) was injected into the column. After injection, PBS buffer was flushed into the column to promote cell rolling on the surface. The flow rate of PBS was optimized by experimentation. The eluted cell suspension was then collected from the end of the column; collected volume of each fraction was 50 μL. The numbers and surface marker profiles of the eluted cells were analyzed using FACS.

Rolling velocity of the KG-1a cells

The microfluidic device was purchased from ibidi GmbH (Model ib80501; ibidi GmbH, Martinsired, Germany). The dimensions of the microfluidic channel were 24 mm (length) × 500 μm (width) × 300 μm (height), with one inlet and one outlet. Anti-CD34 antibody was immobilized on the channel surface, and the modification method used was the same as that used for the tubular column. The cell suspension (2×10^6 cells/mL) was injected into the inlet at a rate of 50 μL/min, and cell rolling was recorded using a high-speed CCD camera (EM-CCD digital camera; Hamamatsu,

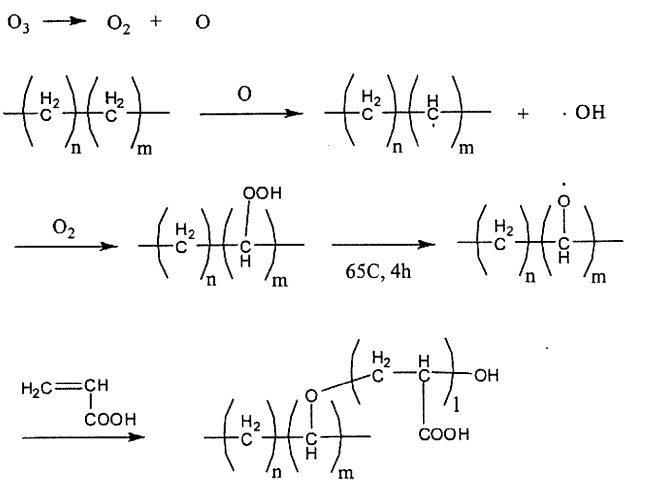

Figure 1. Graft polymerization of acrylic acid on the polyethylene tube.

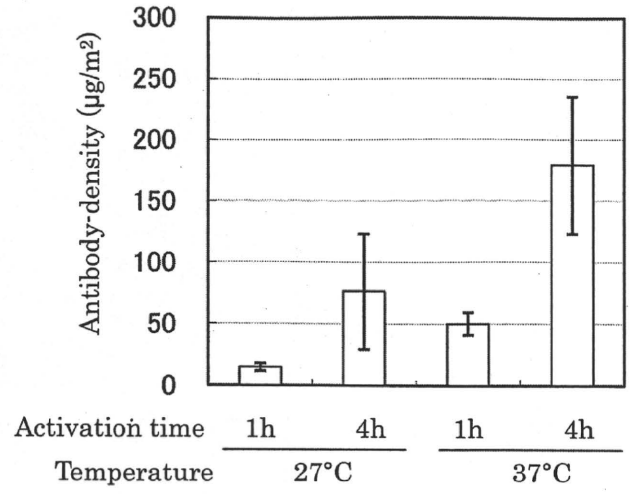

Figure 2. Effects of reaction conditions on immobilized antibody density.

The degree of immobilization is substantially affected by the duration and temperature of the WSC activation reaction. Each data point represents the results of three independent experiments. Data are presented as means ± standard error on the mean.

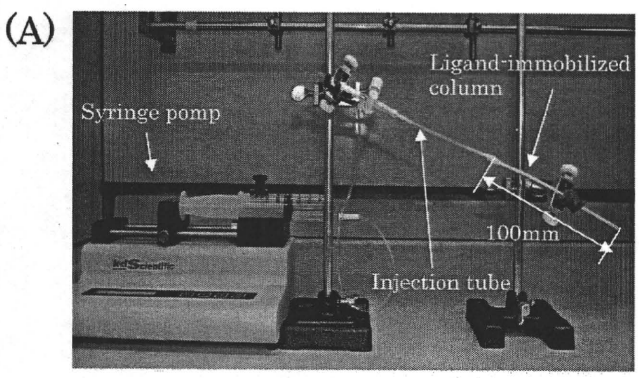

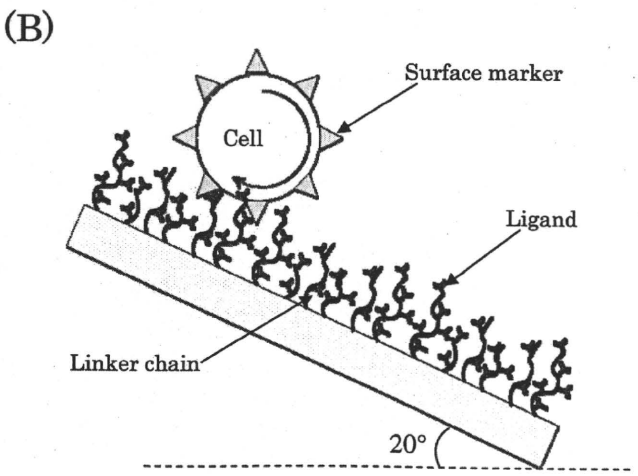

Figure 3. (A) Photograph of the cell separation column system. The antibody-immobilized column was connected to the injection tube and syringe pump. Cells were injected into the injection tube and PBS continuously flowed into the column. The eluted fraction was collected at the end of the column. (B) Schematic diagram of cell rolling on the antibody-immobilized column.

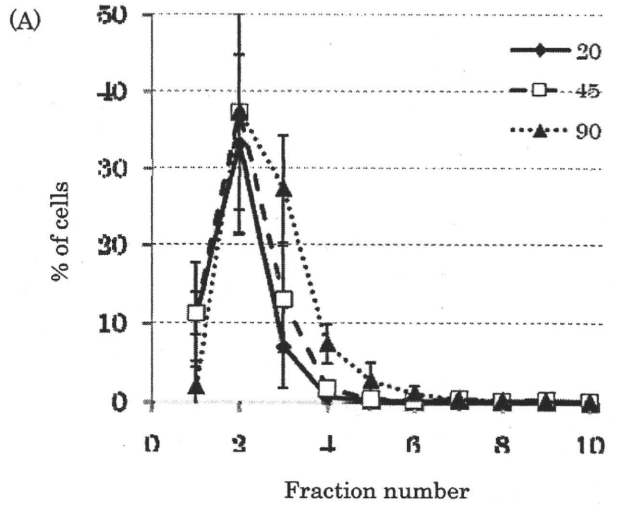

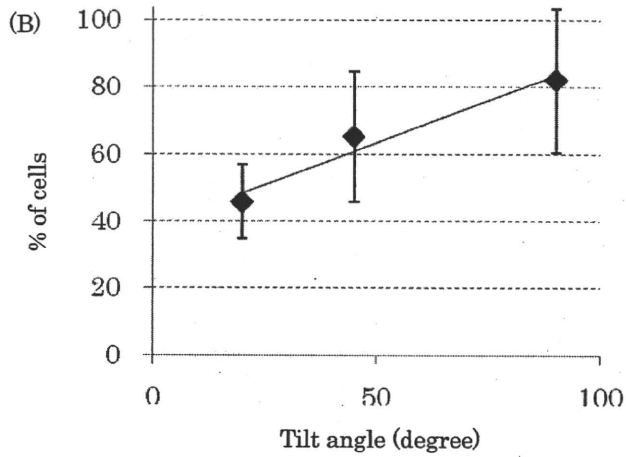

Figure 4. (A) Elution pattern for KG-1a cells at different tilt angles of the antibody-immobilized column, and (B) elution yield of injected KG-1a cells. The vertical axis has been normalized to the total number of injected KG-1a cells. Each data point represents the results of three independent experiments.

Hamamatsu city, Japan). The motion and velocity were analyzed using a personal computer.

FACS analysis

Isolated cells were incubated with FITC-conjugated anti-human CD34 monoclonal antibody (BD Bioscience, San Diego, CA) in PBS for 30 min at 4°C and analyzed using a FACS-Calibur Flow Cytometer (BD Bioscience, San Jose, CA).

Results and Discussion

Fabrication of the antibody-immobilized column

Ozone-induced graft polymerization is effective for polyethylene matrices with a fine structure because ozone gas can be charged into the inner surface and peroxides can be uniformly introduced. The reaction mechanism is shown in Figure 1. The surface concentration of peroxide and its reaction mechanism with vinyl monomer have been previously reported.[33,34] The introduction of the graft polymer chain was confirmed by toluidine blue staining. When the polymer

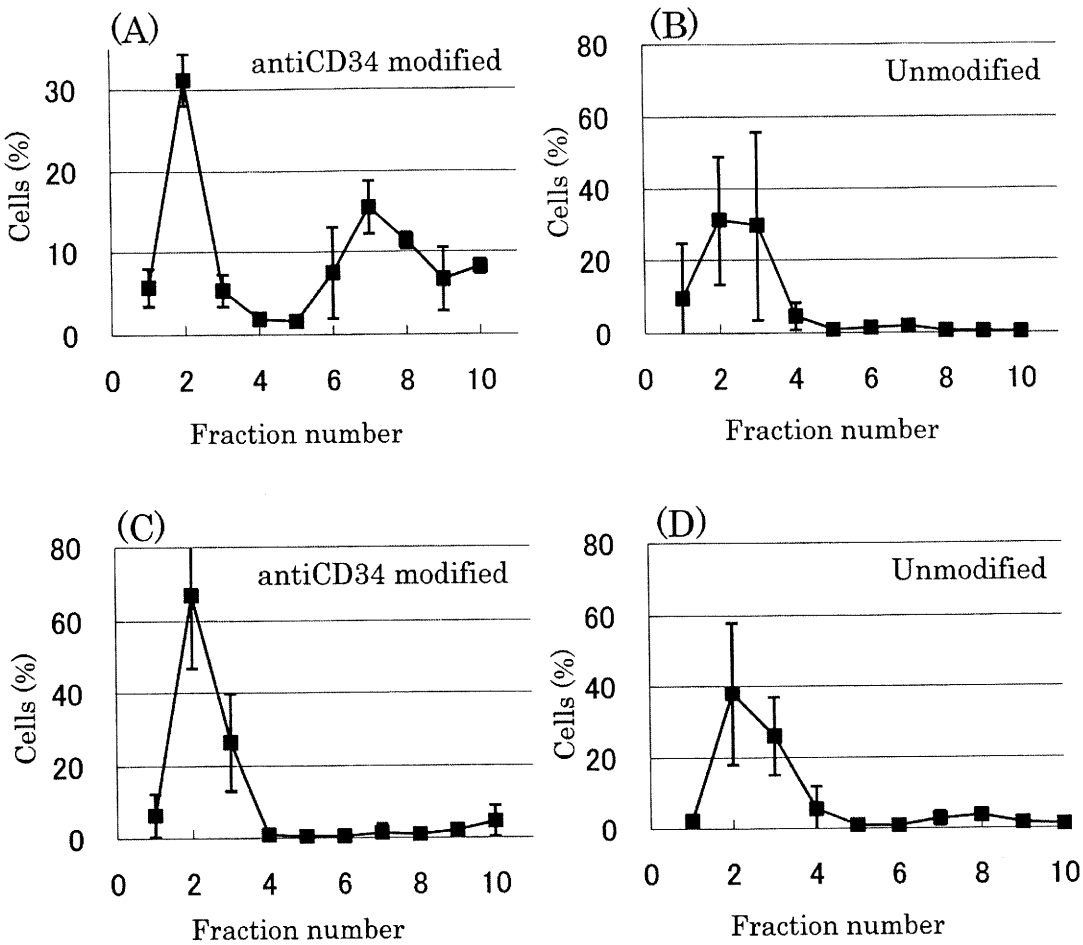

Figure 5. Elution profiles for KG-1a (A and B) and HL-60 cells (C and D) on the anti-CD34 modified column (A and C) and unmodified column (B and D).

The vertical axis has been normalized to the total number of cells. Fifty microliters of the cell suspension was applied and 50 μL of the eluant was collected in each fraction. The cell numbers in each fraction were analyzed using FACSCalibur flow cytometry. Each data point represents the results of 3 independent experiments; the data are presented as means ± standard error on the mean.

concentration was 30%, it was more difficult to flash medium inside the column compared with the lower concentrations. Therefore, a column reacted with 20% acrylic acid solution was selected for the subsequent experiments.

To develop a high-performance column for separating cells with various surface marker densities, the density of the immobilized anti-CD34 antibody should be well controlled. To optimize conditions for antibody immobilization on the inner surface of the tube, we measured the density of the immobilized antibody using HRP-labeled anti-mouse IgG goat antibody. Figure 2 shows the effects of temperature and the WSC activation period on the immobilized density of the anti-CD34 antibody. At an activation temperature of 27°C, the antibody could not be immobilized to the graft chain. On the other hand, when the reaction mixture was incubated at 37°C, the density of the immobilized antibody was approximately 180 $\mu g/m^2$ or about 1.2×10^9 mol/m^2. Cell rolling adhesion is defined as the continuous interaction between a ligand and the cell surface.[18] Rolling velocity is largely restricted by the ligand density and the interaction with the surface marker. Greenberg reported that 10^9 mol/m^2 (800 sites/μm^2) was suitable for cell rolling on a ligand-modified substrate in an experimental as well as theoretical study.[22] In our experiments, the anti-CD34 antibody density in the area occupied by a single cell was 6.3×10^4 sites/cell, and the antibody density was nearly the same as that in Greenberg's report. On the basis of QuantiBrite PE analysis, Zborowski and coworkers reported that Jurkat cells expressed a high number of CD45 surface antigens with a density of 9×10^4 sites/cell,[35] consistent with the present study. On the basis of our results and those of previous study, the density of the immobilized antibody appears appropriate for cell rolling on the surface.

Column setting

Column settings for cell rolling are shown in Figure 3. The elution profile and elution yield of the injected KG-1a cells were evaluated on the anti-CD34 immobilized column at a tilt of 20, 45, and 90 degrees and a moderate flow rate of 50 μL/min. Because the cells frequently interacted strongly with the surface antibodies through multivalent interactions, cell elution using a nontilted column was very complicated, despite increasing the flow rate up to 1 mL/min (data not shown). Thereafter, we tilted the column and evaluated the elution profile. Elution patterns for the KG-1a cells at various tilt angles of the column were almost the same, with a single elution peak observed at Fraction 2 (Figure 4A). The injected cells were almost completely eluted without any surface interactions at an angle of 90 degrees. However, the total recovery ratio of the injected cells decreased with decrease in tilt angle (Figure 4B). When the column

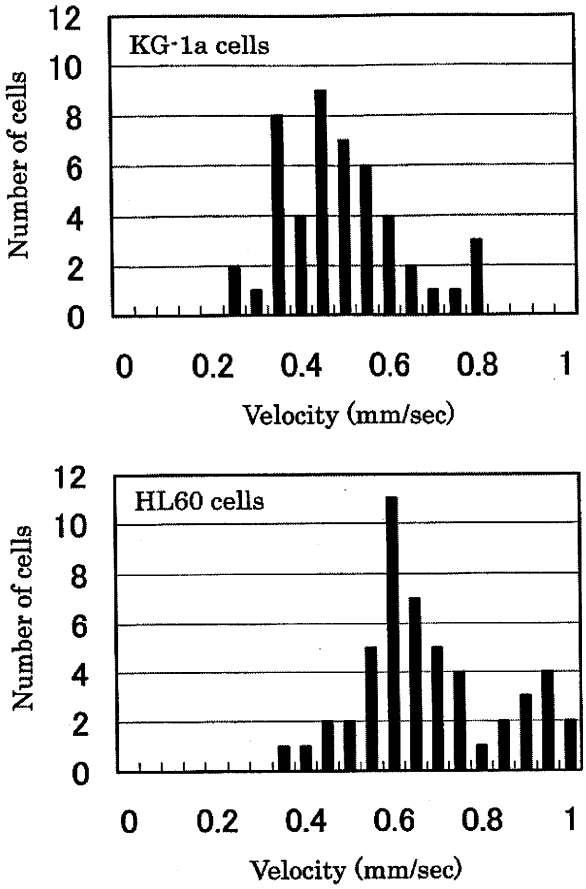

Figure 6. Distributions of the rolling velocities of KG-1a and HL-60 cells on the anti-CD34 antibody immobilized surface. Rolling cells were monitored using a high-speed CCD camera.

angle was 20 degrees, half of the injected cells remained in the column. It is likely that these cells interacted with the surface antibodies, thereby greatly reducing the rolling velocity. After flushing at 50 μL/min, the flow rate was changed to 600 μL/min and most of the injected cells were eluted. We tilted the column angle to 20 degrees, and thus, the cells that interacted with the antibody-immobilized surface rolled on the surface with higher velocity because of the increase in the flow rate. The initial flow rate was maintained at 50 μL/min through Fraction 5, and the rate was changed to 600 μL/min thereafter.

Specificity of the separation profile

KG-1a cells could be separated using the antiCD34 antibody-immobilized column with the settings described earlier. A bimodal elution pattern was observed (Figure 5A). The first elution peak corresponded to the single peak in Figure 4A, suggesting that the cells in the first peak did not interact with the immobilized antibody. In contrast, the delayed fraction was not observed when the KG-1a cells were injected into the unmodified column (Figure 5B). Elution profiles for HL-60 cells (CD34-negative) were compared with those for the CD34-positive cells. All injected HL-60 cells were eluted from the anti-CD34 antibody-immobilized and unmodified column in Fractions 1–3 (Figure 5C,D). This elution profile was the same as the pattern resulting from the column angle fixed at 90 degrees (Figure 4A); that is, HL60 cells injected into the column did not interact with the immobilized antibody. This indicates that the retention time of the cells in the delayed fraction depends on the specific interaction between the surface marker and the immobilized antibody (Supporting Information).

Additional evidence of successful cell separation using the cell rolling mechanism on the column was provided by observation of the rolling velocities on the antibody-immobilized surface. We used a microfluidic channel to measure the distribution of rolling velocities. The microfluidic channel, which was modified with anti-CD34 antibody in the same manner as the column, was set on a microscopy stage, and cell rolling was monitored using a high-speed CCD camera at a moderate flow rate of 50 μL/min. Some cells adhered onto the antibody-immobilized surface and were not able to flow again after adhesion due to multivalent interaction between the cell surface and immobilized antibody. The velocities of the KG-1a and HL-60 rolling cells on the anti-CD34 antibody-immobilized microchannel were 0.45 mm/s and 0.6 mm/s, respectively (Figure 6). Conditions for measurement of the cell rolling velocity on the microscope were different from the cell separation experiments, because the microfluidic device was placed on the flat stage of the microscope without a tilt angle. Under these conditions, large differences in rolling velocity between KG-1a and HL-60 cells were not observed (Figure 6). However, the distributions of the velocities were distinctly different between the KG-1a and HL-60 cells. The difference in the interactions is likely reflected in the velocity distributions. Thus, the velocity of cells rolling was largely dependent on the cell surface marker.

Hammer et al. reported that the rolling velocity of saturated sLe^x-modified polystyrene microspheres was 20 times slower than that of microspheres with a low surface density of sLe^x on an L-selectin coated surface; this difference could be successfully exploited for separation.[8,9] However, it was also reported that CD34-positive bone marrow cells rolled only twice as slowly as CD34-negative cells on an L-selectin modified surface. We observed similar differences in rolling velocities between CD34-positive and -negative cells on the antibody-immobilized surfaces. This small difference in the rolling velocity on a flat microfluidic device prevented cell separation, as shown in Figure 5. We optimized a variety of separation conditions such as consideration of the surface modification tendency, changes in the medium flow rate, and modifying the column setting conditions; this resulted in the bimodal pattern shown in Figure 5A. In our system, separation of rolling cells was most effective after optimization of the column tilt angle and flow rate.

Surface marker characteristics of the isolated cells

To confirm whether our column could be used to separate cells based on CD34 surface density, the CD34 expression level of the KG-1a cells in each fraction was investigated by dual dimensional FACS analysis. Forward-light scatter characteristics (FSC) depend on cell size, which is related to cell cycle or cell proliferation. Fluorescence intensity, indicating the CD34 expression level of each cell line for fractions 2 and 7, is shown in Figure 7A. Two populations of KG-1a were identified by the FACS analysis of CD34 expression versus FSC signal. Although a single population was indicated by the FACS data for Fraction 2, two cell populations (Populations 1 and 2) were observed in Fraction 7. The CD34 expression level of Population 1 was nearly the same as for Population 2, but the cell size of Population 2 was

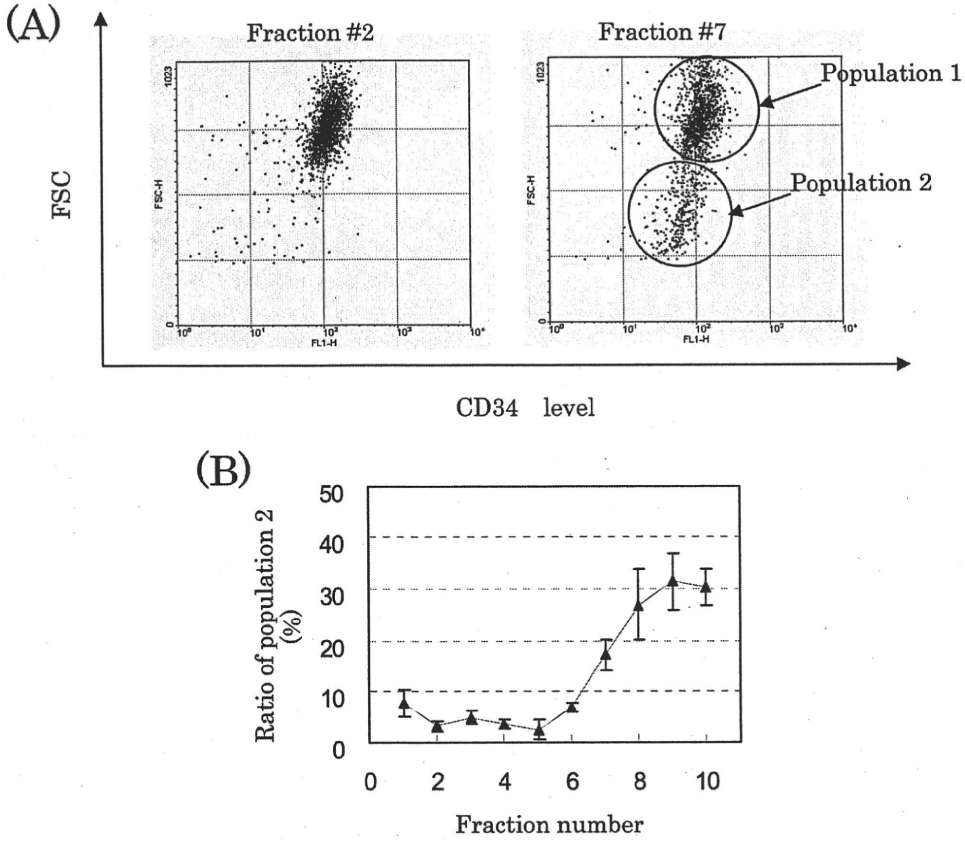

Figure 7. Analysis of the surface marker density of isolated KG-1a cells on the anti-CD34 antibody immobilized column.

(A) Dual dimensional analysis of the CD34 expression level and FSC of the isolated KG-1a cells in Fractions 2 and 7. (B) Ratio of the cells with population producing a high concentration of CD34 in each fraction. Each data point represents the results of three independent experiments.

about half of Population 1. Therefore, the density of CD34 in Population 2 was about 4 times higher than that of Population 1. In Fraction 2, a majority of the cells were of Population 1 as the cell rolling velocity was much larger than for Population 2. The population of the CD34-dense populations was plotted against the fraction number (Figure 7B), and gradually increased with elution time. If the cells in the delayed fraction were separated by static adhesion onto the surface, the high CD34-expression population could not have been isolated from the CD34-positive cell population, because all of the injected cells would have adhered to the resulting surface (Figure 4A). These findings suggest that the cells in the delayed fraction rolled more slowly on the surface than the cells in the previous fractions in a marker-specific manner under shear flow conditions. Thus, this separation procedure is able to isolate cell populations with different marker densities in a continuous manner.

Conclusions

Development of an effective cell separation system is crucial for cell transplantation and for the fundamental study of cell biology. In many cases, negative or positive selection has been used as an effective strategy for cell separation, and the MACS system is a suitable technology for conducting the selection. However, this system cannot separate cells with different densities of surface markers. On the other hand, FACS system can separate cells based on the marker expression level, cellular density, and cell size. For these reasons, FACS was effective in separating the cells in Population 1 and 2 of the KG-1a cells. In this study, we demonstrated the feasibility of a novel cell-separation column that isolates cells through the cell rolling process based on surface marker density under labeling-free conditions. In the standard FACS system, the cells would be exposed to strong media flow, and its velocity and antibody labeling would reduce its viability. To improve the purity of the cells isolated by the column, it is necessary to optimize the surface antibody modification and column structure.

Our system offers several advantages over conventional methods. We would expect cell separation to be more rapid than with conventional methods; moreover, an antibody-immobilized column would likely reduce the degree of cellular damage because cell modification using fluorescence- or magnetic beads-labeled antibodies is unnecessary. For the same reason, the cells thus purified are free of contamination. A highly purified cell population without such impurities or additives will provide an important tool for both transplantation therapy and fundamental study.

Acknowledgments

This work was supported by the Research Grant for Cardiovascular Disease (18A-2) from the Ministry of Health, Labour and Welfare & Grant-in-Aid for Scientific Research on Innovative Areas (20106014).

Literature Cited

1. Stamm C, Westphal B, Kleine HD, Petzsch M, Kittner C, Klinge H, Schumichen C, Nienaber CA, Freund M, Steinhoff G. Autologous bone-marrow stem-cell transplantation for myocardial regeneration. *Lancet*. 2003;361:45–46.

2. Pittenger MF, Martin BJ. Mesenchymal stem cells and their potential as cardiac therapeutics. *Circ Res.* 2004;95:9–20.
3. Noishiki Y, Tomizawa Y, Yamane Y, Matsumoto A. Autocrine angiogenic vascular prosthesis with bone marrow transplantation. *Nat Med.* 1996;2:90–93.
4. Shin'oka T, Imai Y, Ikada Y. Transplantation of a tissue-engineered pulmonary artery. *N Engl J Med.* 2001;344:532–533.
5. Gronthos S, Zannettino ACW, Hay SJ, Shi S, Graves SE, Kortesidis A, Simmons PJ. Molecular and cellular characterisation of highly purified stromal stem cells derived from human bone marrow. *J Cell Sci.* 2003;116:1827–1835.
6. Hung S-C, Chen N-j, Hsieh S-L, Li H, Ma H-L, Lo W-H. Isolation characterization of size-sieved stem cells from human bone marrow. *Stem Cells.* 2002;20:249–258.
7. Pittenger MF, Mackay AM, Beck SC, Jaiswal RK, Douglas R, Mosca JD, Moorman MA, Simonetti DW, Craig S, Marshark DR. Multilineage potential of adult human mesenchymal stem cells. *Science.* 1999;284:143–147.
8. Reyes M, Lund T, Lenvik T, Aguiar D, Koodie K, Verfaillie CM. Purification and ex vivo expansion of postnatal human marrow mesodermal progenitor cells. *Blood.* 2001;98:2615–2625.
9. Jiang Y, Jahagirdar BN, Reinhardt RL, Schwartz RE, Keene CD, Ortiz-Gonzalez XR, Reyes M, Lenvik T, Lund T, Blackstad M, Du J, Aldrich S, Lisberg A, Low WC, Largaespada DA, Verfaillie CM. Pluripotency of mesenchymal stem cells derived from adult marrow. *Nature.* 2002;418:41–49.
10. Baddoo M, Hill K, Wilkinson R, Gaupp D, Hughes C, Kopen GC, Phinney DG. Characterization of mesenchymal stem cell isolated from murine bone marrow by negative selection. *J Cell Biochem.* 2003;89:1235–1249.
11. Gojo S, Gojo N, Takeda Y, Mori T, Abe H, Kyo S, Hata J, Umezawa A. In vivo cardiovasculogenesis by direct injection of isolated adult mesenchymal stem cells. *Exp Cell Res.* 2003; 288:51–59.
12. Tropel P, Noël D, Platet N, Legrand P, Benabid AL, Berger F. Isolation and characterisation of mesenchymal stem cells from adult mouse bone marrow. *Exp Cell Res.* 2004;295:395–406.
13. Rafii S, Lyden D. Therapeutic stem and progenitor cell transplantation for organ vascularization and regeneration. *Nat Med.* 2003;9:702–712.
14. Ziegler BL, Valtieri M, Porada GA, De Maria R, Muller R, Masella B, Gabbianelli M, Casella I, Pelosi E, Bock T, Peschle C. KDR receptor: a key marker defining hematopoietic stem cells. *Science.* 1999;285:1553–1558.
15. Li Y, Zhang C, Xiong F, Yu MJ, Peng FL, Shang YC, Zhao CP, Xu YF, Liu ZS, Zhou C, Wu JL. Comparative study of mesenchymal stem cells from C57BL/10 and mdx mice. *BMC Cell Biol.* 2008;9:24.
16. Jankowski RJ, Deasy BM, Cao B, Gates C, Huard J. The role of CD34 expression and cellular fusion in the regeneration capacity of myogenic progenitor cells. *J Cell Sci.* 2002;115: 4361–4374.
17. Matsuoka S, Ebihara Y, Xu M, Ishii T, Sugiyama D, Yoshino H, Ueda T, Manabe A, Tanaka R, Ikeda Y, Nakahata T, Tsuji K. CD34 expression on long-term repopulating hematopoietic stem cells changes during developmental stages. *Blood.* 2001; 97:419–425.
18. Von Andrian UH, Chambers JD, Mcevoy LM, Bargatze RF, Arfors KE, Butcher EC. Two-step model of leukocyte-endothelial cell interaction in inflammation: distinct roles for LECAM-1 and the leukocyte beta 2 integrins in vivo. *Proc Natl Acad Sci USA.* 1991;88:7538–7542.
19. Hammer DA, Lauffenburger DA. A dynamical model for receptor-mediated cell adhesion to surfaces. *Biophys J.* 1987;52: 475–487.
20. Cozens-Roberts C, Quinn JA, Lauffenberger DA. Receptor-mediated adhesion phenomena. Model studies with the radial-flow detachment assay. *Biophys J.* 1990;58:107–125.
21. Reinhardt PH, Kubes P. Differential leukocyte recruitment from whole blood via endothelial adhesion molecules under shear conditions. *Blood.* 1998;92:4691–4699.
22. Greenberg AW, Kerr WG, Hammer DA. Relationship between selectin-mediated rolling of hematopoietic stem and progenitor cells and progression in hematopoietic development. *Blood.* 2000;95:478–486.
23. Greenberg AW, Brunk DK, Hammer DA. Cell-free rolling mediated by L-selectin and sialyl Lewis(x) reveals the shear threshold effect. *Biophys J.* 2000;79:2391–2402.
24. King MR, Hammer DA. Multiparticle adhesive dynamics. Interactions between stably rolling cells. *Biophys J.* 2001; 81:799–813.
25. Hanley WD, Wirtz D, Konstantopoulos K. Distinct kinetic and mechanical properties govern selectin-leukocyte interactions. *J Cell Sci.* 2004;117:2503–2511.
26. Salimi-Moosavi H, Szarka R, Andersson P, Smith R, Harrison DJ. Biology Lab-on-a-Chip for Drug Screening, Canada. *Proccedings Micro Total Analysis Systems '98.* 1998.
27. Omolola Eniola A, Hammer DA. In vitro characterization of leukocyte mimetic for targeting therapeutics to the endothelium using two receptors. *Biomaterials.* 2005;26:7136–7144.
28. Greenberg AW, Hammer DA. Cell separation mediated by differential rolling adhesion. *Biotechnol Bioeng.* 2001;73:111–124.
29. Chang WC, Lee LP, Liepmann D. Biomimetic technique for adhesion-based collection and separation of cells in a microfluidic channel. *Lab Chip.* 2005;5:64–73.
30. Fu AY, Spence C, Scherer A, Arnold FH, Quake SR. A microfabricated fluorescence-activated cell sorter. *Nat Biotechnol.* 1999;17:1109–1111.
31. Miwa J, Suzuki Y, Kasagi N. Adhesion-based cell velocity regulation in an antibody-coated micro column for stem cell separation. In: *Nineth International Conference in Miniaturezed System Chemistry and Life Science,* Boston; 2005:868–870.
32. Karnik R, Hong S, Zhang H, Mei Y, Anderson DG, Karp JM, Langer R. Nanomechanical control of cell rolling in two dimensions through surface patterning of receptors. *Nano Lett.* 2008; 8:1153–1158.
33. Fujimoto K, Takebayashi Y, Inoue H, Ikada Y. Ozone-induced graft polymerization onto polymer surface. *J Polym Sci Part A: Polym Chem.* 1993;31:1035–1043.
34. Yamauchi J, Yamaoka A, Ikemoto J, Matsui T. Graft copolymerization of methyl methacrylate onto polypropylene oxidized with ozone. *J Polym Sci Part A: Polym Chem.* 1991;43:1197–1203.
35. Schneider T, Moore LR, Jing Y, Haam S, Williams PS, Fleischman AJ, Roy S, Chalmers JJ, Zborowski M. Continuous flow magnetic cell fractionation based on antigen expression level. *J Biochem Biophys Methods.* 2006;68:1–21.

Manuscript received Apr. 23, 2009, and revision received Aug. 18, 2009.

TISSUE ENGINEERING: Part C
Volume 00, Number 00, 2010
© Mary Ann Liebert, Inc.
DOI: 10.1089/ten.tec.2009.0218

Methods Article

A Suspension Induction for Myocardial Differentiation of Rat Mesenchymal Stem Cells on Various Extracellular Matrix Proteins

Azizi Miskon, M.Eng.,[1–3] Atsushi Mahara, Ph.D.,[1] Hiroshi Uyama, Ph.D.,[2] and Tetsuji Yamaoka, Ph.D.[1,4]

The microenvironment of bone marrow-derived mesenchymal stem cells (MSCs) strictly regulates their differentiation. In this study, we have developed a new suspension induction method for myocardial differentiation of bone marrow-derived rat MSCs (rMSCs) *in vitro* on various extracellular matrix (ECM) proteins. Myocardial differentiation of rMSCs was induced with a conventional monolayer method and our suspension method. In our suspension induction, a cell suspension was treated with the medium in the presence of an inducer, incubated for 2 h under a suspension conditions, and moved to a monolayer culture on gelatin-coated, collagen type I-coated, fibronectin-coated, or polystyrene dishes until the total induction time was 24 h. We evaluated the myocardial differentiation by counting the number of colonies of beating cells, performing immunohistochemical staining, and measuring the expression of cardiac-specific gene mRNA using real-time quantitative polymerase chain reaction. We found that rMSCs induced with the conventional monolayer method did not differentiate efficiently, whereas beating cell colonies were found on ECM-coated dishes of suspension-induced cells, after 3 weeks of culture, especially on gelatin-coated dishes. The beating cells were positively stained with anti-troponin T-C antibody and expressed specific cardiac markers. In conclusion, these results demonstrated that the suspension induction followed by subsequent culture on gelatin ECM substrates is a promising method for differentiating rMSCs into cardiomyocytes *in vitro*.

Introduction

ISCHEMIC HEART DISEASE is the primary cause of death throughout the world.[1] Adult cardiac muscle, unlike skeletal muscle, lacks the ability to regenerate after ischemic injury. The only eventual therapy is cardiac transplantation. However, this option is limited by a lack of donor organs.

An implantable left ventricular assist device has been proposed as a bridge to transplant for many patients who are on a waiting list for donor organs.[2] Left ventricular assist device can improve organ perfusion, reduce wall stress, and improve functional capacity and quality of life, but it is not an option for the majority of people with heart failure.[3,4] Thus, the ultimate goal is to repair the injured myocardium by cell transplantation.

Some fundamental studies and clinical trials suggest that cell-based therapies can improve cardiac function.[5–8] The isolation of cardiomyocytes from a patient's heart is unrealistic at present. In general, three types of potential cell sources have been proposed, but the search for these sources and types of cells are still under investigation.[9] One potential source is allogeneic cells, including human embryonic stem cells or fetal allogeneic cardiomyocytes, but there remain ethical issues in their use. Another option is transgenic sources. Genetically engineered animal cardiomyocytes have been studied in an attempt to reduce the rejection reaction *in vivo*, which is still a long-term problem in recipients.[9]

To deal with this problem, autograft bone marrow-derived mesenchymal stem cells (MSCs) are foreseen to be the most promising candidate for transplantation, because they are easy to obtain and less immunogenic than other stem cells. The differentiation of MSCs into cardiomyocytes *in vivo* has been observed, but it occurs at an extremely low rate and its efficiency is under debate.[7,10]

The production of autologous beating cardiomyocytes is thus an attractive goal for cell-based therapy. For this purpose, it is preferable to differentiate MSCs into cardiomyocytes

[1]Department of Biomedical Engineering, Advanced Medical Engineering Center, National Cardiovascular Center Research Institute, Osaka, Japan.
[2]Department of Chemical Engineering, Osaka University, Osaka, Japan.
[3]Department of Electronic Engineering, Faculty of Electrical and Electronics Engineering, University Tun Hussein Onn Malaysia, Johor, Malaysia.
[4]JST, CREST, Tokyo, Japan.

in vitro before transplantation, and it is crucial to understand how best to achieve this.

Based on traditional isolation of MSCs and monolayer culture, Wakitani *et al.* reported that rat MSCs (rMSCs) were differentiated to myogenic cells after 24 h of exposure to DNA-demethylating agent 5-azacytidine,[10] and Makino *et al.* reported that the repeated treatment of murine MSCs with 5-azacytidine differentiated the cells into cardiomyocytes with high cardiac marker expression *in vitro*.[11] These findings are in contrast with a report that functional cardiac cells and gene expression were not obtained after treatment with 5-azacytidine.[12] Xu Wang *et al.* also reported cardiac marker expression in 5-azacytidine-treated MSCs, but they did not observe any beating cells.[13] The differences in these observations might be related to the efficiency of the inducer and the timing of induction.

Clemmons *et al.* reported that fibroblasts in the suspension did not undergo DNA synthesis and division.[14] Griffin and Houstan reported that cells in monolayer cultures are in a static environment and have a relatively small surface area for diffusion, in contrast to suspension cultures in which the entire surface area is exposed to the drug.[15] In addition, in suspensions, efflux transporters are not retained because of the loss of cell polarity and redistribution of canalicular membranes[16]; therefore, the compound remains in the cell. Hence, we assumed that by treating the cells with the inducer in suspension culture, the treated cells were more likely to proceed toward the differentiation phase instead of the division phase.

Langer and Vacanti reported that three important components of tissue-engineered constructs were the cell source, soluble chemical factor, and extracellular matrix (ECM).[17] ECM proteins and the cooperation between signaling pathways triggered by soluble factors such as growth and differentiation factors were found to determine cell proliferation and cell differentiation.[18] In our previous study, ECM components were seen to affect the beating behavior of primary neonatal cardiomyocytes and cardiac differentiated P19.CL6 cells in which enhanced beating behavior and cardiac differentiation on gelatin-coated dishes were observed.[19]

The aim of our studies was to produce spontaneously beating cardiac cells from rMSCs by our new induction method on different substrates. Optimal substrates for stem cell attachment, proliferation, and differentiation have been reported for various types of stem cells.[20] In this study, treated rMSCs were cultured on gelatin-coated, fibronectin-coated, collagen type I-coated, and polystyrene dishes. We treated rMSCs using a newly established suspension method, and the differentiation tendency was compared with those treated by the conventional monolayer method.

Materials and Methods

Bone marrow cell preparation

Femora and tibiae of 4-week-old, male Sprague Dawley rats with average body weight of 80 g were collected and adherent soft tissues were removed. Institutional guidelines for the care and use of laboratory animals were observed. The rMSCs were obtained from collected femora and tibiae by flushing the marrow cavities. Isolated cells were cultured in high-glucose Dulbecco's modified Eagle's medium (DMEM-HG; Gibco, Grand Island, NY) supplemented with 10% fetal bovine serum (lot no. 7297H; MP Biomedicals, Eschwege, Germany), 5% heat-inactivated horse serum (lot no. 076K8430; Sigma-Aldrich, St. Louis, MO), and penicillin (100 U/mL)/streptomycin (100 μg/mL) (Wako, Osaka, Japan).

The cells were seeded on 10 mm fibronectin-coated dishes (BD Falcon, BD BioCoat, BD Biosciences, Bedford, MA) and incubated in a 5% carbon dioxide (CO_2)/air atmosphere at 37°C. At 24 h after plating, nonadherent cells were removed, and the medium was changed every 3 days until the adherent cells reached 80% confluence. The cells in one dish were harvested with 0.25 mg/mL trypsin (Lonza, Walkersville, MD), washed with phosphate-buffered saline (PBS), and seeded onto three new dishes.

Isolation of neonatal heart

Cardiomyocytes were isolated from neonatal (2-day-old) Sprague Dawley rat hearts by the collagenase digestion method with modifications.[21,22] Institutional guidelines for the care and use of laboratory animals were followed. The hearts were removed and carefully minced with a scalpel blade into fragments and rinsed several times with Hanks' balanced salt solution (Sigma-Aldrich) to remove blood and cellular debris. The minced hearts were gently stirred in 50 mL collagenase solution (0.15 M NaCl, 5.63 mM KCl, 0.02 M HEPES, 0.02 M $NaHCO_3$, 3.74 mM $CaCl_2 \cdot 2H_2O$, and 6.5×10^4 U collagenase [lot no. 06032W; Wako]) at 37°C for 30 min. The resulting cell suspension was filtered through a 40 μm pore-sized nylon cell strainer (BD Falcon, BD BioCoat, BD Bioscience) and centrifuged at 78 *g* for 3 min.

Isolated cardiomyocytes were cultured in minimum essential medium alpha (Gibco) supplemented with 10% (v/v) fetal bovine serum (lot no. 7297H; MP Biomedicals) and 100 IU/L penicillin–streptomycin (Wako) on 60 mm gelatin-coated dishes (Iwaki; Asahi Glass, Tokyo, Japan). Three days after isolation the mRNA levels of the cardiac marker genes were evaluated.

Cardiomyocyte differentiation

Monolayer induction. The rMSCs at fourth passage were seeded on 60 mm gelatin-coated dishes (Iwaki; Asahi Glass), fibronectin-coated dishes (BD Falcon, BD BioCoat, BD Biosciences), collagen type I-coated dishes, and noncoated polystyrene dishes (Iwaki; Asahi Glass) at a density of 1.0×10^5 cells/dish. The cells were cultured at 37°C in humidified air with 5% CO_2, reaching 80% confluence within 3 days. Afterward the cells were exposed to the inducers, 10 μM 5-azacytidine (Nacalai Tesque, Kyoto, Japan), 300 μM L-ascorbic acid phosphate magnesium salt *n*-hydrate (Wako), and 0.025 μg/mL human basic fibroblast growth factor (Sigma-Aldrich)-containing DMEM-HG for 24 h. Then, the inducers were washed away and cells were cultured for 5 weeks with DMEM-HG without inducers to develop the beating cells. The medium was changed every 3 days. The cell morphologies were observed every day using Nikon Eclipse TE 300 (Nikon, Tokyo, Japan) light microscope. An image was taken after 3 weeks of cultivation using Image Pro 4.5 software (Media Cybernetics, Silver Spring, MD).

Suspension induction. The suspension of 1.0×10^5 rMSCs was treated with and without 10 μM 5-azacytidine (Nacalai

Tesque), 300 μM L-ascorbic acid phosphate magnesium salt *n*-hydrate (Wako), and 0.025 μg/mL human basic fibroblast growth factor (Sigma-Aldrich)-containing DMEM-HG in a floating condition in a centrifuge tube (Iwaki; Asahi Glass) for 2 h at 37°C in humidified air with 5% CO_2. The treated cells were cultured on 60 mm gelatin-coated dishes (Iwaki; Asahi Glass), fibronectin-coated dishes (BD Falcon, BD BioCoat, BD Biosciences), collagen type I-coated dishes, and noncoated polystyrene dishes (Iwaki; Asahi Glass) in the presence of inducers until the total induction time was 24 h, then with DMEM-HG without inducers for 5 weeks. The medium was changed every 3 days. The cell morphologies were examined every day using a Nikon Eclipse TE 300 (Nikon) light microscope. Images were taken after 3 weeks of cultivation using Image Pro 4.5 software (Media Cybernetics).

The experiments were repeated to determine the expression of troponin C type-2 after suspension induction.

Total RNA isolation and reverse transcription

Total cellular RNAs from both noninduced and induced rMSCs with monolayer induction and suspension induction were extracted by QuickGene RNA cultured cell kit S (Fujifilm Life Science, Tokyo, Japan) after 1, 2, and 3 weeks of culture. In another experiment, total cellular RNAs from induced rMSCs with suspension induction were extracted after 1, 2, 3, 4, and 5 weeks. The cellular RNAs from neonatal cardiomyocytes were also extracted with the same protocol after 3 days of culture as a positive control for real-time quantitative polymerase chain reaction (PCR). Total cellular RNAs were calculated as follows: $[RNA] = A_{260}$ (nm)× Dilution×40 μg/mL. The RNAs from beating and nonbeating colonies were extracted separately.

First-strand cDNAs were synthesized using a mixture of oligo$(dT)_{18}$ primer. Total cellular RNAs (200 ng) were incubated with 2.5 μM oligo$(dT)_{18}$ primer at 70°C for 10 min to denature RNA secondary structure and then incubated at 4°C to let the primer anneal to the RNA. A given amount of 5× reverse transcriptase (RT) buffer (Toyobo, Osaka, Japan) and 2.5 mM dNTP mixture (Takara Bio, Shiga, Japan) (4 μL) were added and incubated at 37°C for 5 min. Reverse transcriptase (100 units; Toyobo) was added into the mixture and the RT reaction was extended at 37°C for 1 h. Then the reaction was heated at 94°C for 5 min to inactivate the enzyme and cooled at 4°C for 15 min. RNase (DNase-free, 0.5 μg; Roche Diagnostics GmbH, Mannheim, Germany) was added into the mixture and incubated at 37°C to remove the template RNA. To confirm that the beating cells were cardiomyocytes, an immunochemical study was conducted, in which the expressions of cardiac-specific markers troponin C type 1 (slow, *TNNC 1*), troponin T type 2 (cardiac, *TNNT 2*), troponin I type 3 (cardiac, *TNNI 3*), GATA binding protein 4 (GATA 4), and myocyte enhancer factor 2D (*MEF2D*).

Real-time quantitative PCR

Real-time quantitative PCR was conducted with SYBR Green. Primers for PCR analysis of troponin T type-2 (cardiac, *TNNT 2*), troponin C type-1 (slow, *TNNC 1*), troponin I type-3 (cardiac, *TNNI 3*), *GATA4*, *MEF2D*, and troponin C type-2 (fast, *TNNC 2*) were designed using Primer Express software (Perkin-Elmer Applied Biosystems, Warrington,

TABLE 1. POLYMERASE CHAIN REACTION PRIMERS USED IN THIS STUDY

Genes	*Sense*	*Position (bp)*	*Antisense*	*Position (nt)*	*Accession no.*
TNNT 2	5′-GAAACAGGATCAACGACAACCA-3′	827–848	5′-CGCCCGGTGACTTTGG-3′	875–890	NM_012676
TNNC 1	5′-GATCTCTTCCGCATGTTTGACA-3′	295–316	5′-TGGCCTGCAGCATCATCTT-3′	352–370	NM_001034105
TNNI 3	5′-CCAGGAATCTGCAATCCCATT-3′	65–85	5′-CCGCATCGCTGCTCTCA-3′	114–130	NM_017144
TNNC 2	5′-AGATCGAATCCCTGATGAAGGA-3′	392–413	5′-CATCTTCAGAAACTCGTCGAAGTC-3′	442–465	NM_001037351
GATA 4	5′-CAGTTCTGCACACCTGTATTCCA-3′	452–474	5′-GCTCCCCTTTATTTGCAAGTCA-3′	515–536	NM_144730
MEF2D	5′-GCGGCTGGATACTTGGACATT-3′	1251–1271	5′-CGGTGAGATTGTCAACTCTTCATC-3′	2009–2032	NM_030860
GAPDH	5′-CTACCCCCAATGTATCCGTTGT-3′	742–763	5′-TAGCCCAGGATGCCCTTTAGT-3′	842–862	AB017801

nt, nucleotide.

UK). Primer sequences are shown in Table 1. The reaction mixtures contained 23.74 μL distilled water, 25 μL SYBR Green Real-Time PCR master mix (Toyobo), 100 nM of each primer, and 0.26 μL cDNA. The thermal profile for PCR was 50°C for 2 min, followed by 95°C for 10 min, and then 40 cycles of 15 s at 95°C and 1 min at 60°C. We also performed a negative control PCR reaction using 0.26 μL distilled water to ensure the absence of template contamination in PCR reagents. The cycle number at which the reaction crossed an arbitrarily placed threshold (Cτ) was determined for each gene. The average Cτ values of triplicate measurements were used for all subsequent calculations on the basis of the delta Ct method (ΔCτ). The amount of mRNA levels was determined by $2^{\Delta C\tau}$. To correct any variation in mRNA content, the quantities of the genes of interest were normalized by the quantity of glyceraldehyde-3-phosphate dehydrogenase and expressed as relative values of mRNA.

Immunostaining analysis

To confirm the protein expression in addition to the mRNA expression, cells generated by the monolayer method and beating cells generated by suspension induction were stained with anti-troponin T-C antibody. After 4 weeks of culture, the cells were fixed with 10% formalin in PBS and washed with PBS three times. Next, the cells were incubated for 5 min in 0.1% hydrogen peroxide in PBS to quench endogenous peroxide activity and washed in PBS twice for 5 min each. Then the cells were incubated with 10% Block-Ace™ (Dainippon Sumitomo Pharma, Osaka, Japan) in PBS for 20 min to suppress nonspecific binding of IgG. After three cycles of washing with PBS for 5 min each, the cells were incubated with 2.5 μL/mL primary antibody (troponin T-C(C-19), sc-8121; Santa Cruz Biotechnology, Santa Cruz, CA) for 60 min in PBS with 1.5% Block-Ace™, washed three times in PBS for 5 min, and incubated with 2 μL/mL secondary antibody (donkey anti-goat IgG-FITC, sc-8121; Cosmo Bio, Tokyo, Japan) for 45 min in PBS with 1.5% Block-Ace™. The cells were washed with PBS four times and mounted with aqueous mounting medium.

Stained cells were observed using Nikon Eclipse TE 300 (Nikon) fluorescence microscope. An image was taken using Image Pro 4.5 software (Media Cybernetics) with the following parameters: for bright file, an exposure time of 20 ms and gain of 7; for fluorescence, an exposure time of 2 s and gain of 7.

Statistical analysis

All data are presented as means ± standard deviations. Statistical analysis was performed using Student's *t*-test. A *p*-value of less than 0.05 was considered significant.

Results

rMSCs form myotubes

After 3 weeks of cultivation, the shape of the cells induced with suspension induction was very different from that with monolayer induction, as shown in Figure 1. The shape of the suspension-induced cells appeared to be myotubular and seemed to correlate closely to beating colony formation. The phenotypic difference in these shapes was confirmed by measuring *TNNT 2*, *TNNC 1*, and *TNNC 2* expression.

Expression of cardiomyocyte-associated genes in monolayer and suspension induction

Troponin T type-2 (cardiac, *TNNT 2*) and troponin C type-1 (slow, *TNNC 1*) are known to be markers of cardiomyocytes,[23,24] and troponin C type-2 (fast, *TNNC 2*) is reported to be expressed at the early stage of the cardiac development.[23] In this study, the expression of *TNNT 2* was higher in the suspension induction than in the monolayer induction, as shown in Figure 2A. On the other hand, *TNNC 1* expression was generally lower in the suspension induction than in the monolayer induction (Figure 2B). However, the gene expression of *TNNC 2* was detected only in the suspension induction and not in the monolayer induction (Figure 2C). These results indicate that the suppression of *TNNC 1* may have been affected by the expression of *TNNC 2* and signify

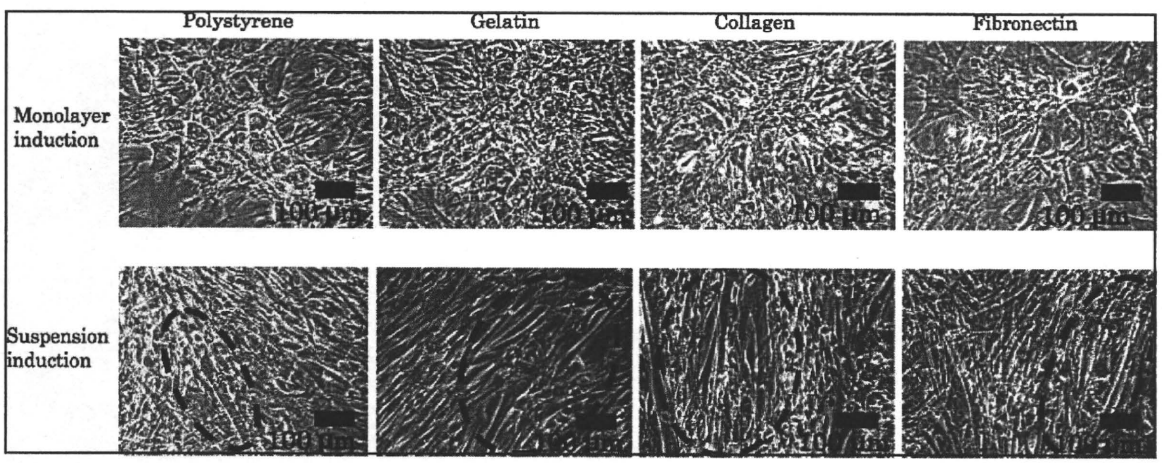

FIG. 1. Microscopic image of rMSCs after monolayer or suspension induction and 3 weeks of culture on several types of dishes. Dashed regions represent the regions of cells with myotube-like shape. rMSC, rat mesenchymal stem cell.

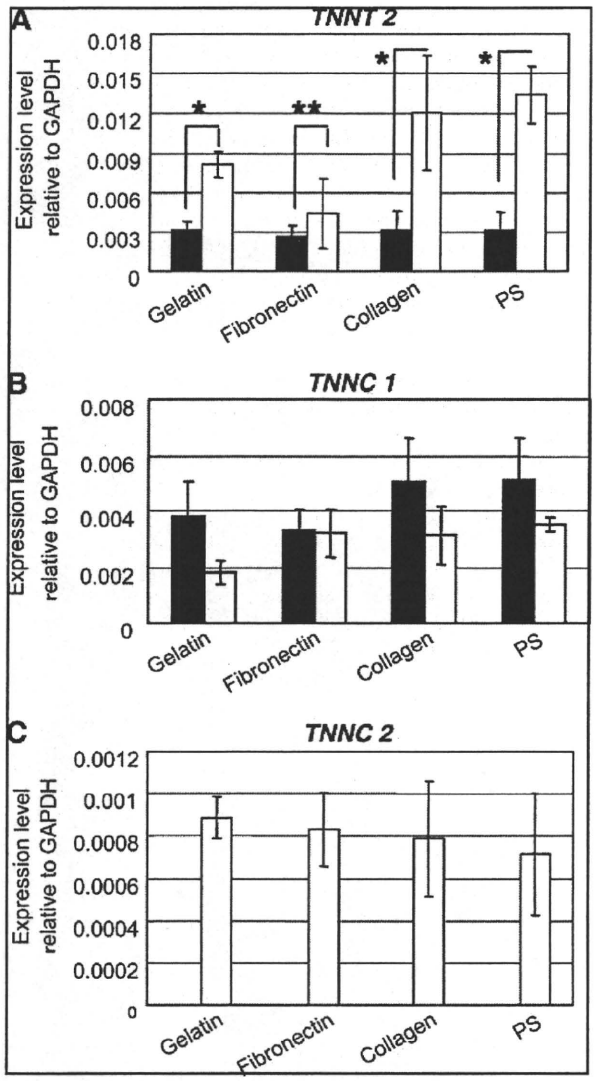

FIG. 2. Expression levels of (A) *TNNT 2*, (B) *TNNC 1*, and (C) *TNNC 2* in cells after monolayer (■) or suspension induction (□) and culture on different extracellular matrix proteins or uncoated polystyrene dishes ($n = 3$; bars represent ± standard deviation; $^{*}p < 0.01$, $^{**}p < 0.16$).

the initial stage of cardiac differentiation, as suggested by Stoutamyer and Dhoot.[23] In addition, the gene expression of *TNNT 2* and *TNNC 2* were detected only in rMSCs treated with inducers and not in the rMSCs treated without inducers (Supplemental Fig. S1 available online at www.liebertonline.com). The expression level of TNNC 1 was generally higher in the treated rMSCs with inducers than in the treated rMSCs without inducers.

In other experiments, the expression of *TNN2* was detected after 2 weeks of differentiation and decreased by culture time as shown in Figure 3. This observation is possibly related to the cardiomyocyte differentiation. Besides, this result shows similarity with that during quail heart development *in ovo*.[23]

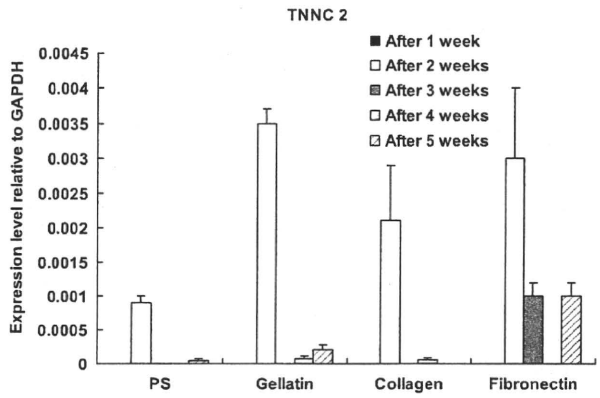

FIG. 3. The expression of *TNNC 2* decreased with culture period. Data are means ± standard deviation; $n = 3$ for each sample.

Myotube-like cells on ECM substrates show spontaneous contraction

In general, about 3 weeks are needed to observe spontaneous beating of the cells without the addition of any chemical reagent, such as acetylcholine.[10,25] Once the beatings are detected, it takes about another 1 week to enter the synchronous stage.

Interestingly, the beating cells and colonies were detected only after they were induced with suspension induction on ECM protein-coated dishes, but not in monolayer induction. We carried out these induction experiments 14 times and found a beating colony only once in monolayer induction on gelatin-coated dishes. As five dishes were used for each experiment, the average number of beating colonies in one dish was calculated as 0.75 ± 1.5 (Table 2). However, the real probability of beating colony appearance was much lower than this value. A large number of beating colonies (4.5 ± 0.6) with sizes ranging from 400 to 500 μm were found in the five gelatin-coated dishes, and 1.3 ± 1.5 beating colonies with a similar size were found in the five fibronectin-coated and collagen type-I-coated dishes. No beating cells were detected in noncoated polystyrene dishes in either form of induction. Table 2 summarizes the colonies of beating cells. Supplemental Video S1 (available online at www.liebertonline.com) shows the beating colonies after 4 weeks of culture on gelatin-coated dishes.

In some cases, monolayer-treated and suspension-treated rMSCs were detached from the dishes after 3 weeks of culture.

TABLE 2. AVERAGE NUMBER OF BEATING COLONIES FOUND IN A DISH (n = 5)

	Average number of beating colonies per dish	
Dish type	*Monolayer*	*Suspension*
Gelatin	0.75 ± 1.5	4.5 ± 0.6
Fibronectin	0	1.3 ± 1.5
Collagen type I	0	1.3 ± 1.5
Polystyrene	0	0

Five 60 mm culture dishes were used for calculation of average beating colony number.